**Figure 2.** Bacterial adhesion to the cell clump. A flow test was performed with *A. actinomycetemcomitans* LPS-stimulated RAW 264.7 cells for 120 min, followed by *S. sanguinis* SK36-GFP and *S. sanguinis* SK36 Δpili-GFP. Black and white bars indicate *S. sanguinis* SK36-GFP and SK36 Δpili-GFP, respectively. *Significant difference between mean of adhesion ratios of the groups assessed by Tukey-Kramer HSD test (*$p < 0.05$).
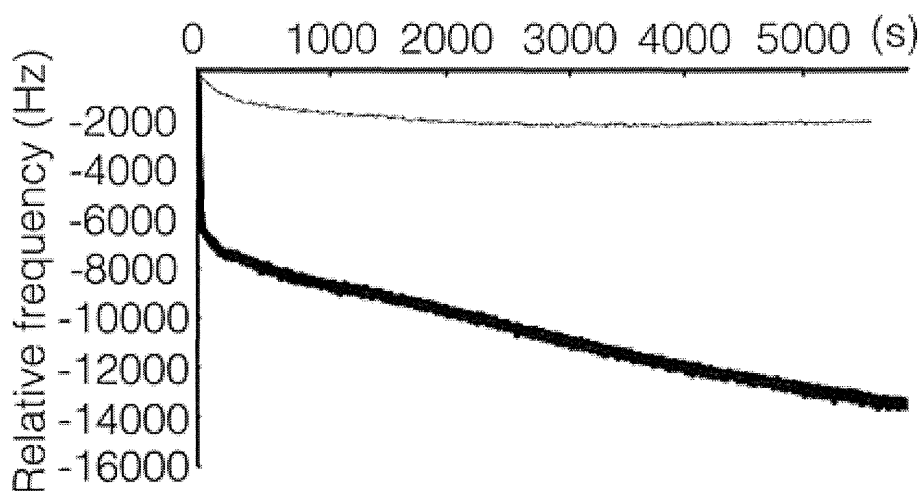


**Figure 3.** Interaction between *S. sanguinis* pili and ICAM-1. ICAM-1 was immobilized directly on a QCM ceramic sensor chip soaked in PBS at 25°C. *S. sanguinis* SK36 (bold black line) and *S. sanguinis* Δpili (black line) organisms were applied to the equilibrated solution as described in Materials and Methods.

interaction enhances cell-to-cell aggregation, suggesting that pili and ICAM-1 are involved in infective endocarditis caused by *S. sanguinis* via interaction of these molecules. It has been reported that *S. sanguinis* may be associated with infective endocarditis (Ge et al., 2008; Herzberg et al., 1992) and that periodontopathic bacteria are related to coronary heart disease (Brodala et al., 2005; Sakurai et al., 2007; Spahr et al., 2006). Njoroge et al. (1997) showed that *Porphyromonas gingivalis* fimbriae are required for adherence to and invasion of oral epithelial cells, while another group reported that adhesion of monocytes to vascular endothelial cells is an important step in atherosclerosis (Libby et al., 2002). We consider that our novel microchannel chip system provides the ability to verify adhesion of periodontopathic bacteria such as *P. gingivalis* with vascular endothelial cells. Conclusively, in the present study, we found it to be quite useful for *in vitro* observations of the process of adhesion of bacteria to macrophage cell clumps.

## ACKNOWLEDGEMENT

## REFERENCES

Avandhanula V, Rodriguez CA, Ulett GC, Bakaletz LO, Adderson EE (2006). Nontypeable *Haemophilus influenzae* Adheres to Intercellular Adhesion Molecule 1(ICAM-1) on Respiratory Epithelial Cells And Upregulates ICAM-1 Expression. Infect. Immun. **74**(2):830-838.

Barrau K, Boukamery A, Imbert G, Casalta JP, Habib G, Messana T, Bonnet JL, Rubinstein E, Raoult D (2004). Causative organisms of infective endocarditis according to host status. Clin. Microbiol. Infect. **10**(4):302-308.

Brodala N, Merricks EP, Bellinger DA, Damrongsri D, Offenbacher S, Beck J, Madianos P, Sotres D, Chang YL, Koch G (2005). *Porphyromonas gingivalis* Bacteremia Induces Coronary and Aortic Atherosclerosis in Normocholesterolemic and Hypercholesterolemic pigs. Arterioscler. Thromb. Vasc. Biol. **25**(7):1446-1451.

Chen YY, LeBlanc DJ (1992). Genetic analysis of scrA and scrB from *Streptococcus sobrinus* 6715. Infect. Immun. **60**(9):3739-3746.

Douglas CW, Heath J, Hampton KK, Preston FE (1993). Identity of viridans streptococci isolated from cases of infective endocarditis. J. Med. Microbiol. **39**(3):179-182.

Ge X, Kitten T, Chen Z, Lee SP, Munro CL, Xu P (2008). Identification of *Streptococcus sanguinis* Genes Required for Biofilm Formation and Examination of Their Role in Endocarditis Virulence. Infect. Immun. **76**(6):2551-2559.

Herzberg MC, MacFarlane GD, Gong K, Armstrong NN, Witt AR, Erickson PR, Meyer MW (1992). The Platelet Interactivity Phenotype of *Streptococcus sanguis* Influences the Course of Experimental Endocarditis. Infect. Immun. **60**(11):4809-4818.

Inaba H, Amano A (2010). Roles of Oral Bacteria in

Cardiovascular Diseases – From Molecular Mechanisms to Clinical Cases: Implication of Periodontal Diseases in Development of Systemic Diseases. J. Pharmacol. Sci. **113**(2): 103-109.

Isoda T, Tsutsumi T, Yamazaki K, Nishihara T (2009). Measurement of plaque-forming macrophages activated by lipopolysaccharide in a micro-channel chip. J. Periodont. Res. **44**(5):609-615.

Libby P, Ridker PM, Maseri A (2002). Inflammation and Atherosclerosis. Circulation. **105**(9):1135-1143.

Li X, Kolltveit KM, Tronstad L, Olsen I (2000). Systemic Diseases Caused by Oral Infection. Clin. Microbiol. Rev. **13**(4):547-558.

Nishihara T, Fujiwara T, Koga T, Hamada S (1986). Chemical composition and immunobiological properties of lipopolysaccharide and lipid-associated proteoglycan from *Actinobacillus actinomycetemcomitans*. J. Periodont. Res. **21**(5): 521-530.

Njoroge T, Genco RJ, Sojar HT, Hamada N, Genco CA (1997). A Role for Fimbriae in *Porphyromonas gingivalis* Invasion of Oral Epithelial Cells. Infect. Immun. **65**(5):1980-1984.

Okahashi N, Nakata M, Sakurai A, Terao Y, Hoshino T, Yamaguchi M, Isoda R, Sumitomo T, Nakano K, Kawabata S, Ooshima T (2010). Pili of *Streptococcus sanguinis* bind to fibronectin and contribute to cell adhesion. Biochem. Biophys. Res. Commun. **391**(2):1192-1196.

Okahashi N, Nakata M, Terao Y, Isoda R, Sakurai A, Sumitomo T, Yamaguchi M, Kimura RK, Oiki E, Kawabata S, Ooshima T (2011). Pili of *Streptococcus sanguinis* bind to salivary amylase and promote the biofilm formation. Microb. Pathog. **50**(3-4):148-154.

Paik S, Senty L, Das S, Noe JC, Munro CL, Kitten T (2005). Identification of Virulence Determinants For Endocarditis in *Streptococcus sanguinis* by Signature-Tagged Mutagenesis. Infect. Immun. **73**(9):6064-6074.

Roberts GJ (1999). Dentists are innocent! "Everyday" bacteremia is the real culprit: a review and assessment of the evidence that dental surgical procedures are a principal cause of bacterial endocarditis in children. Pediatr. Cardiol. **20**(5):317-325.

Sakurai K, Wang D, Suzuki J, Umeda M, Nagasawa T, Izumi Y, Ishikawa I, Isobe M (2007). High Incidence of *Actinobacillus actinomycetemcomitans* Infection in Acute Coronary Syndrome. Int. Heart. J. **48**(6):663-675.

Shay K (2002). Infectious Complications of Dental and Periodontal Diseases in the Elderly Population. Clin. Infect. Dis. **34**(9):1215-1223.

Spahr A, Klein E, Khuseyinova N, Boeckh C, Muche R, Kunze M, Rothenbacher D, Pezeshki G, Hoffmeister A, Koenig W (2006). Periodontal infections and coronary heart disease: role of periodontal bacteria and importance of total pathogen burden in the Coronary Event and Periodontal Disease (CORODONT) study. Arch. Intern. Med. **166**(5):554-559.

Telford JL, Barocchi MA, Margarit I, Rappuoli R, Grandi G (2006). Pili in Gram-positive pathogens. Nat. Rev. Microbiol. **4**(7):509-519.

Tsutsumi T, Nakashima K, Isoda T, Yokota M, Nishihara T (2010). Involvement of adhesion molecule in *in vitro* plaque-like formation of macrophages stimulated with *Aggregatibacter actinomycetemcomitans* lipopolysaccharide. J. Periodont. Res. **45**(4):550-556.

# Osteoarthritis and Cartilage

OARSI OSTEOARTHRITIS RESEARCH SOCIETY INTERNATIONAL

# High molecular weight hyaluronic acid regulates osteoclast formation by inhibiting receptor activator of NF-κB ligand through Rho kinase

CrossMark

W. Ariyoshi [†], T. Okinaga [†], C.B. Knudson [‡], W. Knudson [‡], T. Nishihara [†*]

† Division of Infections and Molecular Biology, Department of Health Promotion, Kyushu Dental University, Kitakyushu, Fukuoka, Japan
‡ Department of Anatomy and Cell Biology, The Brody School of Medicine, East Carolina University, Greenville, NC, USA

## ARTICLE INFO

## SUMMARY

Objective: To determine the effects of high molecular weight hyaluronic acid (HMW-HA) on osteoclast differentiation by monocytes co-cultured with stromal cells.
Methods: Mouse bone marrow stromal cell line ST2 cells were incubated with HMW-HA or 4-methylunbeliferone (4-MU) for various times. In some experiments, cells were pre-treated with the anti-CD44 monoclonal antibody (CD44 mAb) or Rho kinase pathway inhibitors (simvastatin or Y27632), then treated with HMW-HA. The expression of receptor activator of NF-κB ligand (RANKL) was determined using real-time reverse transcription polymerase chain reaction (RT-PCR), western blotting, and immunofluorescence microscopy, while the amount of active RhoA was measured by a pull-down assay. To further clarify the role of HMW-HA in osteoclastogenesis, mouse monocyte RAW 264.7 cells were co-cultured with ST2 cells pre-stimulated with $1,25(OH)_2D_3$. Osteoclast-like cells were detected by staining with tartrate-resistant acid phosphatase (TRAP).
Results: HMW-HA decreased RANKL mRNA and protein expressions, whereas inhibition of hyaluronic acid (HA) synthesis by 4-MU enhanced RANKL expression. Blockage of HA-CD44 binding by CD44 mAb suppressed HMW-HA-mediated inhibition of RANKL. Pull-down assay findings also revealed that HMW-HA transiently activated RhoA in ST2 cells and pre-treatment with CD44 mAb inhibited the activation of RhoA protein mediated by HMW-HA. Moreover pre-treatment with Rho kinase pathway inhibitors also blocked the inhibition of RANKL by HMW-HA. Co-culture system results showed that HMW-HA down-regulated differentiation into osteoclast-like cells by RAW 264.7 cells induced by $1,25(OH)_2D_3$-stimulated ST2 cells.
Conclusions: These results indicated that HA-CD44 interactions down-regulate RANKL expression and osteoclastogenesis via activation of the Rho kinase pathway.

## Introduction

Hyaluronan, or hyaluronic acid (HA), is an unsulfated long polysaccharide chain comprised of repeating disaccharide units of N-acetylglucosamine and glucuronic acid, and a major component of the extracellular matrix (ECM). HA is present with a high molecular mass in mammalian bone marrow and connective tissues, as well as skin, vitreous humor of the eye, cartilage, and umbilical cord tissue. Unlike other glycosaminoglycans, it is synthesized as a free polysaccharide, rather than substituted on a core protein, and newly synthesized HA polymers of 2,500–25,000 repeating disaccharides have a molecular mass ranging from $10^3$–$10^4$ kDa. The roles of HA range from purely structural functions to regulation of several cellular responses including proliferation, differentiation, motility, adhesion and gene expression.[1,2]

High molecular weight hyaluronic acid (HMW-HA) is clinically used as a symptom- or disease-modifying drug for non-surgical treatments of joints as well as cartilage diseases such as osteoarthritis (OA)[3], as the efficacy of articular HA therapy for OA has been demonstrated in animal experimental models[4,5] and clinical trials[6,7]. Although the underlying mechanisms may be due to its chondroprotective and anti-inflammatory effects, the precise roles of HA in the pathogenesis of OA remain largely unknown.

Many connective tissue cells exhibit a large HA and proteoglycan-rich pericellular matrix that is tethered to the cell surface via interactions with the HA receptor CD44[8], a

* Address correspondence and reprint requests to: T. Nishihara, 2-6-1 Manazuru, Kokurakita-ku, Kitakyushu 803-8580, Japan. Tel: 81-93-285-3050; Fax: 81-93-581-4984.
E-mail addresses: arikichi@kyu-dent.ac.jp (W. Ariyoshi), t-oki@kyu-dent.ac.jp (T. Okinaga), knudsonc@ecu.edu (C.B. Knudson), knudsonw@ecu.edu (W. Knudson), tatsujin@kyu-dent.ac.jp (T. Nishihara).

multifunctional transmembrane glycoprotein that exhibits extensive molecular heterogeneity. The CD44 ectodomain is responsible for the binding of HA, while the cytoplasmic domain regulates specific signaling such as RhoA-activated Rho kinase[9], Rho/Rac1-specific guanine nucleotide exchange factors (p115RhoGEF[10], Tiam1[11], and Vav2[12]), c-Src kinase[13], and transforming growth factor-β receptors[14]. CD44 also directly binds to cytoskeletal proteins such as ankyrin and ERM (ezrin, radixin, moesin).[15]

Bone remodeling is a highly regulated process involving the coordinated action of osteoblasts and osteoclasts. Osteoclasts originate from hematopoietic precursors of a monocyte/macrophage lineage and differentiate into multinucleated giant cells specialized to resorb bone by fusion of mononuclear progenitors[16]. It has also been shown that osteoclast precursors must interact with osteoblasts/stromal cells to differentiate into mature osteoclasts[17], while osteoclast formation is induced in the presence of the receptor activator of the NF-κB ligand (RANKL), a member of the tumor necrosis factor (TNF) superfamily, which is expressed by osteoblasts/bone stromal cells. RANKL interacts with the osteoclast cell surface receptor RANK, which in turn recruits TNF receptor-associated factors (TRAFs)[18], and plays a crucial role in the osteoclast differentiation axis.

It is possible that receptor-mediated effects of HA and derivatives lead to changes in the metabolism of chondrocytes[19,20], synoviocytes[21,22], and subchondral bone osteoblasts[23], and several researchers have reported the involvement of HA in osteoclast formation and resorption[24,25]. In a previous study, we demonstrated that low molecular weight HA (LMW-HA, molecular weight <8 kDa) enhanced both osteoclast formation and function in vitro[26]. However, scant attention has been given to the effects of HMW-HA on osteoclast-supporting cells. In the present study, we examined the effects of HMW-HA on osteoclastogenesis and found that it suppressed osteoclast formation via down-regulation of RANKL in bone marrow derived osteoblastic/stromal cells in vitro.

## Methods

### Reagents and antibodies

High molecular weight HA (HMW-HA, molecular weight 2,500 kDa) was supplied by Seikagaku Corp. (Tokyo, Japan), while 4-methylumberlliferone (4-MU) was purchased from Sigma–Aldrich (St. Louis, MO, USA). The anti-RANKL polyclonal antibody was obtained from R&D Systems Inc. (Minneapolis, MN, USA), anti-β-actin monoclonal antibody from Sigma–Aldrich and anti-RhoA monoclonal antibody from Cell Signaling Technology Inc. (Beverly, MA, USA).

### Cell cultures

Mouse bone marrow stromal cells ST2 was obtained from Riken Cell Bank (Ibaraki, Japan) and maintained in alpha-minimum essential medium (α-MEM; GIBCO, Grand Island, NY, USA) supplemented with 10% fetal calf serum (FCS; Sigma–Aldrich), 100 U/ml penicillin G (Meiji Seika Pharm Co., Tokyo, Japan), and 100 μg/ml streptomycin (Wako Pure Chemical Industries, Osaka, Japan) at 37°C in an atmosphere of 5% $CO_2$. ST2 cells were incubated with HMW-HA or 4-MU for various times. For some experiments, cells were pre-treated with the anti-CD44 monoclonal antibody (10 μg/ml, Calbiochem, San Diego, CA, USA), simvastatin (10 μM, Sigma–Aldrich), or Y27632 (10 μM, Calbiochem), then treated with HMW-HA (50 μg/ml) in the continuing presence or absence of each reagent.

### Detection of cell surface HA and RANKL

ST2 cells were treated in 8-well chamber slides ($5 \times 10^3$ cells/well), then fixed with 4% paraformaldehyde in phosphate buffered saline (PBS, pH 7.4) for 1 h, quenched with 0.2 M glycine in PBS, and blocked with 1% bovine serum albumin (BSA, Sigma–Aldrich) in PBS for 1 h. For HA detection, the cells were incubated with 2.0 μg/ml of a biotinylated-HA binding protein (HABP) probe (Seikagaku Corp.) overnight at 4°C. Following extensive washing, the cells were incubated with 1 μg/ml neutravidin-fluorescein isothiocyanate (FITC) (1:1,000) (Invitrogen, Carlsbad, CA, USA) in PBS containing 1% BSA for 1 h at 4°C.

For immunofluorescence analysis of RANKL, fixed cells were incubated overnight with the anti-RANKL antibody (1:100), then for 1 h at room temperature with FITC conjugated anti-goat IgG (Santa Cruz Biotechnology, Santa Cruz, CA, USA). To visualize stress fibers, cells were incubated with rhodamine phalloidin (Invitrogen) for 20 min at room temperature, then washed, mounted in mounting medium containing the nuclear stain, 4'6-diamidino-2-phenylindole dihydrochloride (DAPI; Vector Laboratories Inc., Burlingame, CA, USA), and visualized using a Fluorescence Microscope BZ-9000 (Keyence Corp., Osaka, Japan). Images were captured digitally in real time and processed using BZ-II imaging software (Keyence Corp.).

### Quantitative real-time reverse transcription polymerase chain reaction (RT-PCR)

Total RNA was isolated from cells with TRIzol reagent (Invitrogen). Samples were reverse transcribed with q-Srcipt cDNA Supermix reagents (Quanta BioSciences, Gaithersburg, MD, USA) and amplified for 30 min at 42°C. For real-time RT-PCR, the PCR products were detected using FAST® SYBR Green Master Mix (Applied Biosystems, Foster City, CA, USA) using the following primer sequences: Gapdh forward; 5'-GACGGCCGCATCTTCTTGA-3' and reverse; 5'-CACACCGACCTTCACCATTTT-3', and Rankl forward; 5'-GGCCAC AGCGCTTCTCA-3' and reverse; 5'-CCTCGCTGGGCCA-CATC-3'. Thermal cycling and fluorescence detection were performed using a StepOne™ Real-Time System (Applied Biosystems). Real-time RT-PCR efficiency for each primer set was calculated according to the method of Rasmussen et al.[27] The fold increase in copy numbers of mRNA was calculated as the relative ratio of the Rankl gene to Gapdh, following the model of Pfaffl.[28]

### Western blot analysis

Following incubation, total protein was extracted using Cell Lysis Buffer (Cell Signaling Technology) containing a protease inhibitor cocktail (Thermo Fisher Scientific, Waltham, MA, USA) and protein contents were measured using a DC protein assay kit (Bio-Rad, Hercules, CA, USA). Twenty micrograms of total protein per sample was loaded and separated on a Mini-PROTEAN TGX 4–15% gradient SDS-PAGE gel (Bio-Rad), then transferred onto polyvinylidene difluoride membranes (Millipore Corp., Bedford, MA, USA). Nonspecific binding sites were blocked by immersing the membranes in 5% skim milk in PBS for 1 h at room temperature. Membranes were subjected to incubation overnight with diluted primary antibodies at 4°C, followed by horseradish peroxidase (HRP) conjugated secondary antibodies for 1 h at room temperature. After washing the membranes, chemiluminescence was produced using ECL reagent (Amersham Pharmacia Biotech, Uppsala, Sweden) and detected digitally with a GelDoc™ XR Plus System (Bio-Rad). Goat anti-RANKL and mouse anti-β-actin were used as the primary antibodies, while HRP-conjugated anti-goat IgG (Santa

Cruz Biotechnology) and anti-mouse IgG (GE Healthcare, Little Chalfont, UK) were used as secondary antibodies.

### RhoA activity

The amount of active RhoA was measured by using a pull-down assay with Rho Assay Reagent (Millipore Corp.), according to the manufacturer's instructions. Briefly, treated cells were washed twice in ice-cold PBS and lysed in lysis buffer (125 mM HEPES pH 7.5, 750 mM NaCl, 5% Igepal CA-630, 50 mM MgCl$_2$, 5 mM EDTA, 10 % glycerol), then the lysates were clarified by centrifugation at 14,000 $\times$ g for 5 min. Thereafter, the supernatant was incubated with Rhotekin-Rho binding domain beads for 45 min with gentle agitation at 4°C, after which the beads were washed 3 times with lysis buffer, followed by re-suspension in 40 μl of Laemmli reducing sample buffer. Precipitated GTP-bound and total RhoA proteins were then analyzed using western blotting analysis with an anti-RhoA monoclonal antibody.

### Osteoclast formation in co-culture system

Osteoclasts were detected by staining with tartrate-resistant acid phosphatase (TRAP) using an Acid Phosphatase Leukocyte Kit (Sigma–Aldrich). In brief, ST2 cells (5 $\times$ 10$^2$ cells/well) were plated in a 96-well plate with αMEM containing 10% FBS and 10$^{-7}$ M 1,25(OH)$_2$D$_3$ (Sigma–Aldrich) in the presence or absence of HMW-HA (50 μg/ml). The next day, mouse monocyte RAW 264.7 cells (Riken Cell Bank, Ibaraki, Japan, 1 $\times$ 10$^3$ cells/well) were overlaid for the co-culture system. After co-culturing for 7 days, adherent cells were fixed and stained for TRAP activity, with TRAP-positive multinucleated cells containing three or more nuclei counted under a microscope as osteoclast-like cells.

### Statistics analysis

All statistics analyses were carried out using JMP® software, version 10.0.2 (SAS Institute Inc., Cary, NC, USA). Each of the data groups was tested by using Shapiro–Wilk test and considered to follow a Gaussian distribution when the $P$-value was greater than 0.05. The Levene's test of homogeneity was used to determine the homogeneity of variance. All data were expressed as mean ± standard deviation and analyzed by one-way analysis if variance (ANOVA) and if significant, followed by the suitable post-test (Dunnett's or Tukey's post-test).

### Results

#### HMW-HA down-regulates RANKL expression

We examined the effects of HMW-HA on RANKL expression in ST2 cells. The binding of HMW-HA (50 μg/ml) was monitored using an HABP probe and time-dependent HA binding could be visualized up to 3 h [Fig. 1(A)]. Primer sets for real-time RT-PCR amplification and quantification of mouse Rankl and Gapdh were designed, and
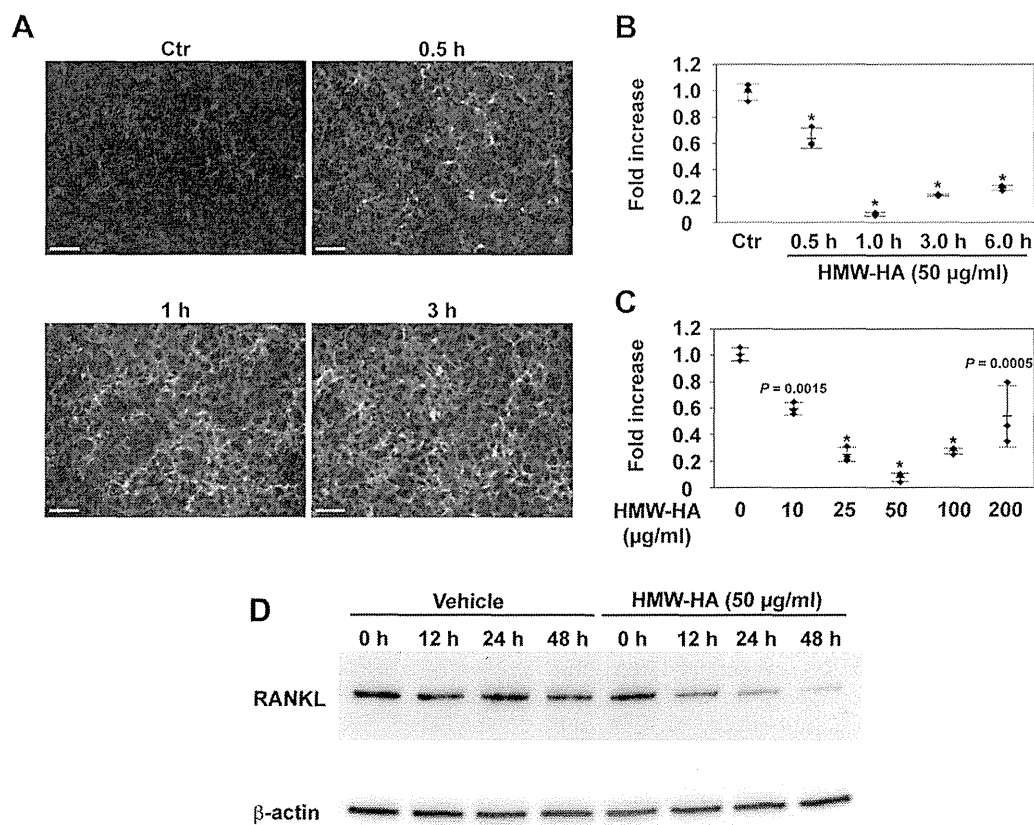


Fig. 1. Effect of HMW-HA on RANKL expression in ST2 cells. ST2 cells were incubated in the presence or absence of HMW-HA for varying times and in various concentrations. (A) Cells were incubated with a biotinylated HABP probe and HA accumulation was visualized using neutravidin-FITC. Bars indicate 10 μm. (B) Time course (ANOVA: $P < 0.0001$) and (C) concentration dependency (ANOVA: $P < 0.0001$) of Rankl mRNA stimulation by HMW-HA was determined by real-time RT-PCR. Data shows the fold changes in Rankl mRNA copy number values from independent samples of $n = 3$, and bars represent means with the standard deviation. Data were analyzed by Dunnett's test after one-way ANOVA. The asterisk indicates $P < 0.0001$ in comparison to control without any treatment. (D) Whole cell lysates were subjected to SDS-PAGE and western blotting analyses, with the blots probed for RANKL. Equivalent protein aliquots of cell lysates were also analyzed for β-actin.

the amplification efficiency of each set was determined, allowing for comparison of mRNA copy numbers between treated and control cultures, which were normalized to Gapdh. After 0.5 h of incubation with HMW-HA, there was a 26.4% decrease in Rankl mRNA copy number as compared to the untreated control cells [Fig. 1(B)]. This effect of HMW-HA was time-dependent, with maximum inhibition observed at the 1-h time point (96.3% inhibition). A concentration-dependent inhibition of Rankl by HMW-HA was also shown [Fig. 1(C)], which reached a maximum at a concentration of 50 μg/ml following 1 h of treatment (93% inhibition). As shown in [Fig. 1(D)], ST2 cell lysates from the control cultures expressed immunoreactive RANKL protein, while treatment with HMW-HA reduced RANKL protein expression in the ST2 cells for up to 48 h.

### 4-MU up-regulates RANKL expression

Next, we investigated whether the receptor-HA pathway has an influence on the expression of RANKL in ST2 cells using 4-MU. It has been reported that 4-MU inhibits HA synthesis and pericellular HA matrix formation in cultured cells.[29,30] We found a time-dependent decrease in accumulation of endogenous HA for up to 6 h following treatment with 4-MU (0.5 mM) [Fig. 2(A)]. Real-time RT-PCR also revealed an 8.1-fold increase in Rankl mRNA copy number as compared to the untreated control cells after 3 h of incubation with HMW-HA [Fig. 2(B)]. This effect of 4-MU was time-dependent, with maximum enhancement observed at the 6-h time point (12.1-fold

increase). In addition, 4-MU induced a concentration-dependent stimulation of Rankl [Fig. 1(C)], with maximum stimulation observed at a concentration of 0.5 mM at 6 h after treatment (9.5-fold increase). Treatment with 4-MU also up-regulated RANKL protein expression in ST2 cells for up to 48 h [Fig. 2(D)].

### Changes in matrix interactions by HA affect RANKL accumulation

ST2 cells at all examined culture times exhibited a background level of RANKL that was primarily localized on the cell surface [Fig. 3(A)]. No immunofluorescent staining was seen with the secondary antibody alone [Fig. 3(B)]. After 24 h of treatment with HMW-HA, RANKL protein accumulation was diminished [Fig. 3(C)]. On the other hand, after 24 h of treatment with 4-MU, RANKL levels were substantially enhanced [Fig. 3(D)].

### CD44 function-blocking monoclonal antibody reverses reduction of RANKL expression induced by HMW-HA

To further examine the role of CD44 as an HA receptor in down-regulation of RANKL, ST2 cells were pre-treated with the CD44 function-blocking monoclonal antibody for 2 h prior to stimulation with HMW-HA. Treatment with the monoclonal antibody inhibited exogenous HMW-HA binding after 1 h of incubation [Fig. 4(A)]. Also, pretreatment with the monoclonal antibody effectively recovered the down-regulation of Rankl mRNA induced by 1 h of treatment with HMW-HA [Fig. 4(B)]. Western blotting analysis
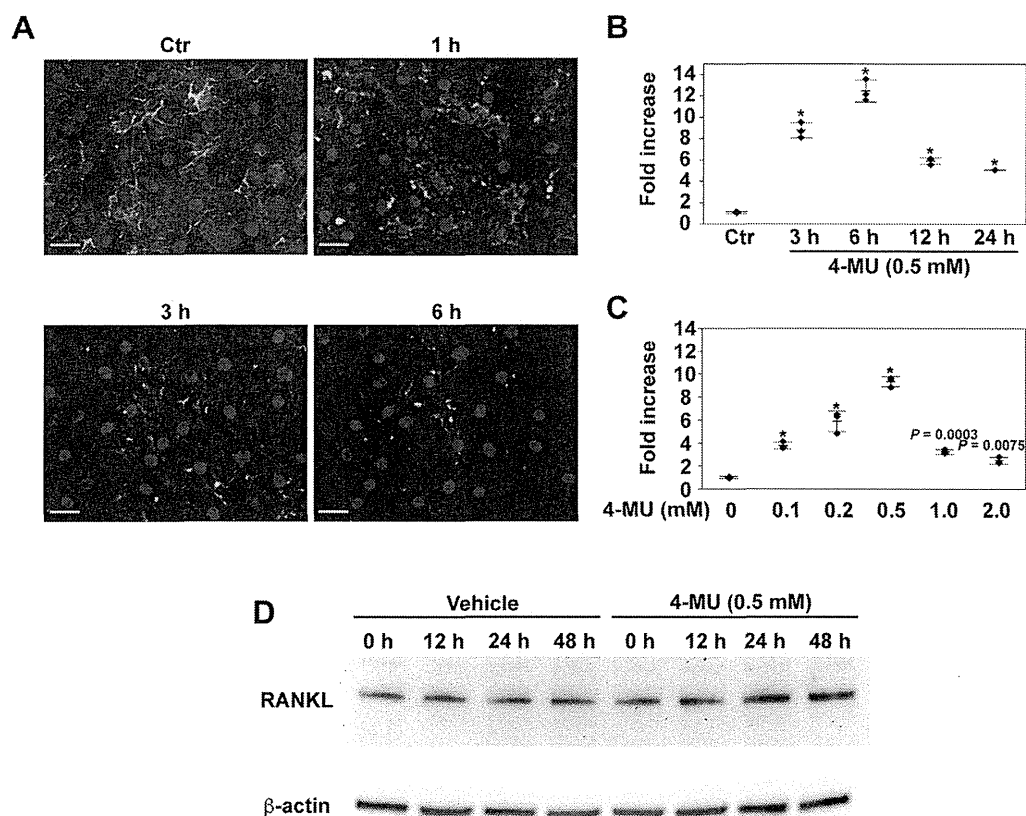


Fig. 2. Effect of 4-MU on RANKL expression in ST2 cells. ST2 cells were incubated in the presence or absence of 4-MU for varying times and in various concentrations. (A) Cells were incubated with a biotinylated HABP probe and HA accumulation was visualized using neutravidin-FITC. Coverslips were mounted in medium containing DAPI. Bars indicate 10 μm. (B) Time course (ANOVA: $P < 0.0001$) and (C) concentration dependency (ANOVA: $P < 0.0001$) of Rankl mRNA stimulation by 4-MU was determined by real-time RT-PCR. Data shows the fold changes in Rankl mRNA copy number values from independent samples of $n = 3$, and bars represent means with the standard deviation. Data were analyzed by Dunnett's test after one-way ANOVA. The asterisk indicates $P < 0.0001$ in comparison to control without any treatment. (D) Whole cell lysates were subjected to SDS-PAGE and western blotting analyses, with the blots probed for RANKL. Equivalent protein aliquots of cell lysates were also analyzed for β-actin.

**Ctr**



**Secondary antibody only**
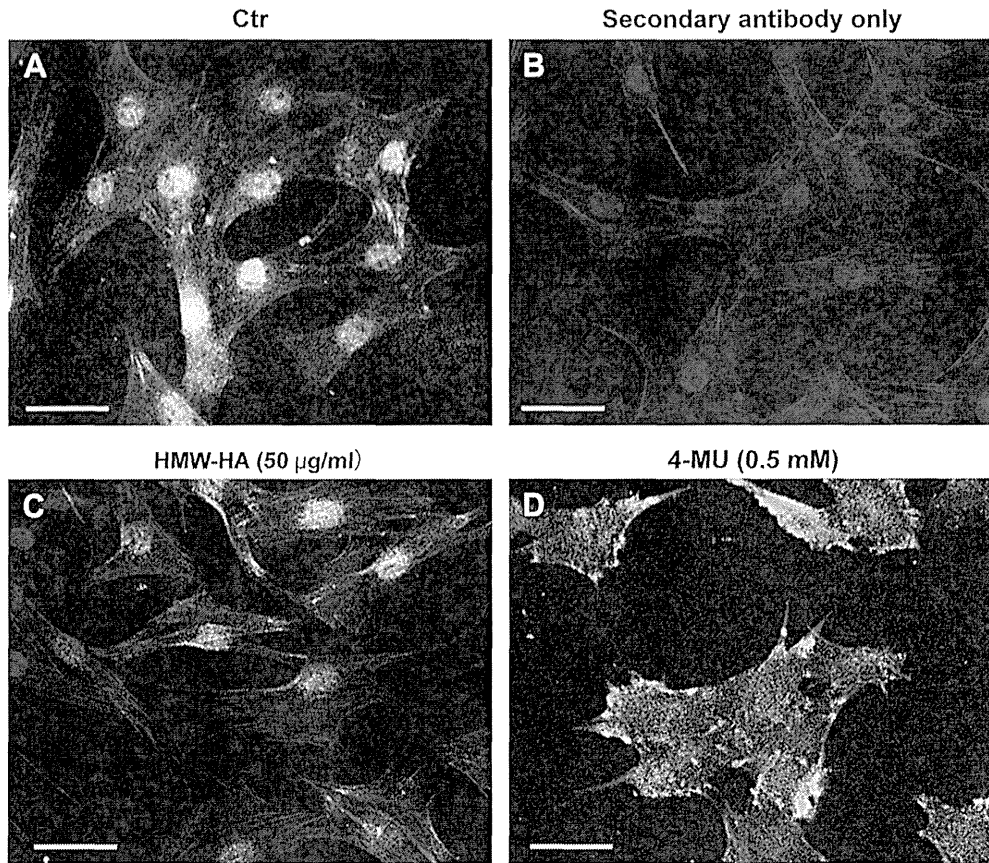
**HMW-HA (50 µg/ml)**

**4-MU (0.5 mM)**

Fig. 3. Effect of HA accumulation on RANKL expression in ST2 cells. ST2 cells were grown on chamber slides, then incubated in the (A) absence or presence (C) of 50 µg/ml of HMW-HA, (D) or 0.5 mM of 4-MU for 24 h. Following treatment, the cells were fixed and immunostained using a polyclonal antibody to detect RANKL and rhodamine isothiocyanate-phalloidin. Coverslips were mounted in medium containing DAPI. (B) Control cells incubated with the secondary antibody alone. Shown are digital overlay images of red, green, and blue fluorescence channels. Bars indicate 20 µm.
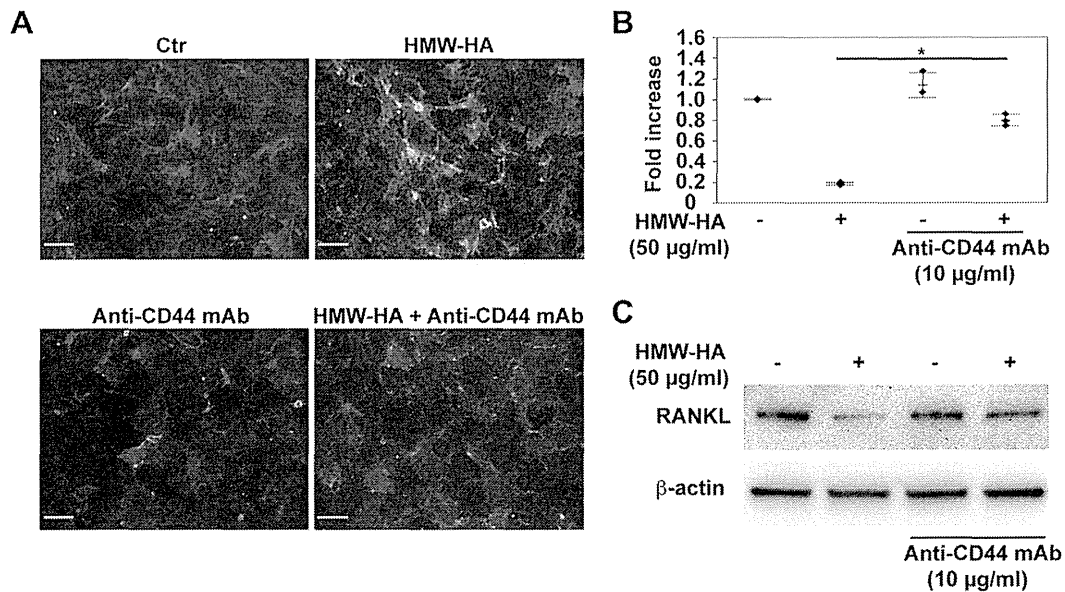


Fig. 4. Effects of CD44 function-blocking antibody on RANKL expression regulated by HMW-HA. ST2 cells were pretreated with or without 10 µg/ml of the CD44 function-blocking monoclonal antibody (CD44 mAb) for 2 h, then incubated in the presence or absence of HMW-HA (50 µg/ml) for the indicated time periods. (A) Cells were incubated with a biotinylated HABP probe and HA accumulation was visualized using neutravidin-FITC. Coverslips were mounted in medium containing DAPI. Bars indicate 10 µm. (B) Total RNA was isolated, and reverse transcribed into cDNA, then PCR amplification was performed using primers specific for *Rankl* and *Gapdh*. Data shows the fold changes in *Rankl* mRNA copy number values from independent samples of $n = 3$, and bars represent means with the standard deviation. Data were analyzed by Tukey's post-test after one-way ANOVA ($P < 0.0001$). The asterisk indicates $P < 0.0001$ in comparison to treatment with HMW-HA. (C) Whole cell lysates were subjected to SDS-PAGE and western blotting analyses, with the blots probed for RANKL. Equivalent protein aliquots of cell lysates were also analyzed for β-actin.

revealed that the monoclonal antibody also recovered the down-regulation of RANKL protein expression mediated after 24 h of incubation with HMW-HA [Fig. 4(C)].

*Interaction between HMW-HA and CD44 induces sequential activation of RhoA protein*

Recent findings indicate that the Rho kinase pathway has important roles in bone metabolism.[31–33] Therefore, we next examined whether HMW-HA induces RhoA activation in ST2 cells. RhoA activity was assessed by detecting GTP-loaded forms of the protein using a pull-down assay. As shown in [Fig. 5(A)], HMW-HA transiently activated RhoA in ST2 cells from 15 to 60 min, while RhoA activity returned to the basal level at 120 min of HMW-HA stimulation. Pre-treatment with the CD44 function-blocking monoclonal antibody inhibited the activation of RhoA protein mediated by HMW-HA stimulation for 30 min [Fig. 5(B)].
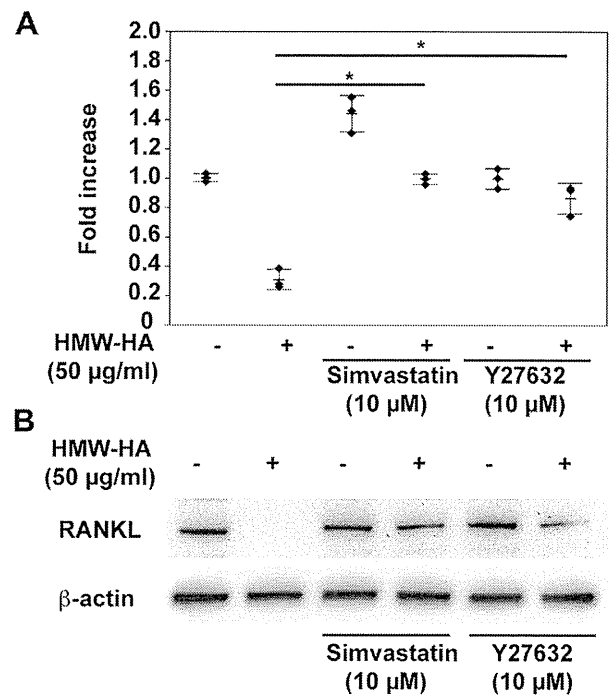
*Rho/ROCK inhibitors attenuate down-regulation of RANKL expression mediated by HMW-HA*

To further examine the role of RhoA activation in HMW-HA-mediated down-regulation of RANKL, ST2 cells were pre-treated with a Rho inhibitor (simvastatin) or selective Rho-associated protein kinase (ROCK) inhibitor (Y27632) for 24 h prior to stimulation with HMW-HA. Pretreatment with these inhibitors effectively blocked the down-regulation of *RANKL* mRNA [Fig. 6(A)] and RANKL protein [Fig. 6(B)] by HMW-HA.

*HMW-HA inhibits osteoclast formation supported by ST2 cells*

To determine whether HMW-HA has an influence ton ST2 cell-supported osteoclast formation, cells were treated with 1,25(OH)$_2$D$_3$, which markedly stimulated *Rankl* mRNA expression in the ST2 cells for up to 24 h, while the addition of HMW-HA decreased the response of the cells to 1,25(OH)$_2$D$_3$ [Fig. 7(A)]. As shown in [Fig. 7(B)], the level of RANKL protein expression was increased in ST2 cells at 48 h after stimulation with 1,25(OH)$_2$D$_3$ and that stimulation was down-regulated by addition of HMW-HA. Western blotting analysis also revealed that pre-treatment with the Rho/ROCK inhibitors attenuated the down-regulation of RANKL protein in 1,25(OH)$_2$D$_3$-stimulated ST2 cells mediated by HMW-HA.

To further clarify the role of the HMW-HA in osteoclastogenesis, we cocultured mouse monocytes (RAW 264.7 cells), as osteoclast precursors with ST2 cells pre-stimulated with 1,25(OH)$_2$D$_3$. As shown in [Fig. 7(C) and (D)], culturing with HMW-HA down-

regulated the differentiation of RAW 264.7 cells into osteoclast-like cells induced by 1,25(OH)$_2$D$_3$-stimulated ST2 cells.

**Discussion**

Bone resorption has been reported to be increased in women with progressive knee OA as compared to those with non-progressive disease[34]. Furthermore, peripheral blood mononuclear cells from patients with OA have been shown to exhibit enhanced capacity to generate osteoclasts and higher levels of bone
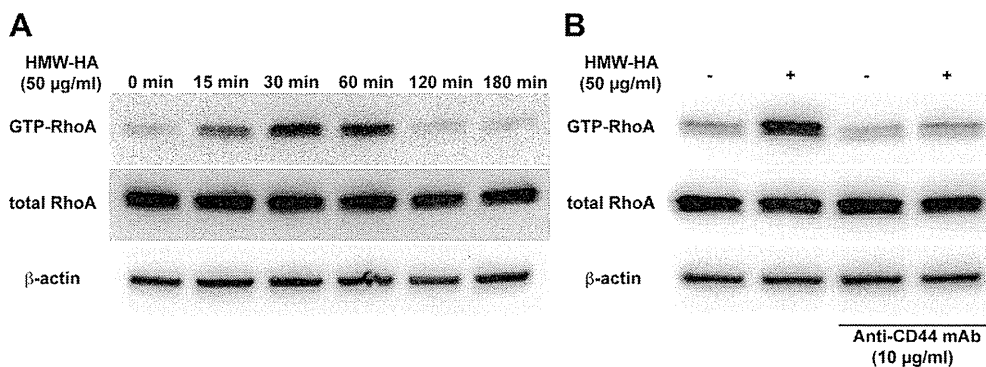


Fig. 6. Effects of RhoA/ROK inhibitors on RANKL expression regulated by HMW-HA. ST2 cells were pretreated with simvastatin (10 μM) or Y27632 (10 μM) for 24 h, then incubated in the presence or absence of HMW-HA (50 μg/ml) for the indicated time periods. (A) Total RNA was isolated, and reverse transcribed into cDNA, then PCR amplification was performed using primers specific for *Rankl* and *Gapdh*. Data shows the fold changes in *Rankl* mRNA copy number values from independent samples of $n = 3$, and bars represent means with the standard deviation. Data were analyzed by Tukey's post-test after one-way ANOVA ($P < 0.0001$). The asterisk indicate $P < 0.0001$ in comparison to treatment with HMW-HA. (B) Whole cell lysates were subjected to SDS-PAGE and western blotting analyses, with the blots probed for RANKL. Equivalent protein aliquots of cell lysates were also analyzed for β-actin.



Fig. 5. Effects of HMW-HA on RhoA activation in ST2 cells. (A) ST2 cells were incubated in the presence or absence of 50 μg/ml of HMW-HA for the indicated time periods. (B) ST2 cells were pretreated with or without 10 μg/ml CD44 mAb for 2 h, then incubated with HMW-HA (50 μg/ml) for 30 min. Whole cell lysates were subjected to SDS-PAGE and western blot analyses, with the blots probed for anti-RhoA (total RhoA). Equivalent protein aliquots of cell lysates were also analyzed for β-actin. GTP-RhoA was isolated utilizing GST-Rhotekin RBD, followed by SDS-PAGE and western blot analyses with the anti-RhoA antibody.
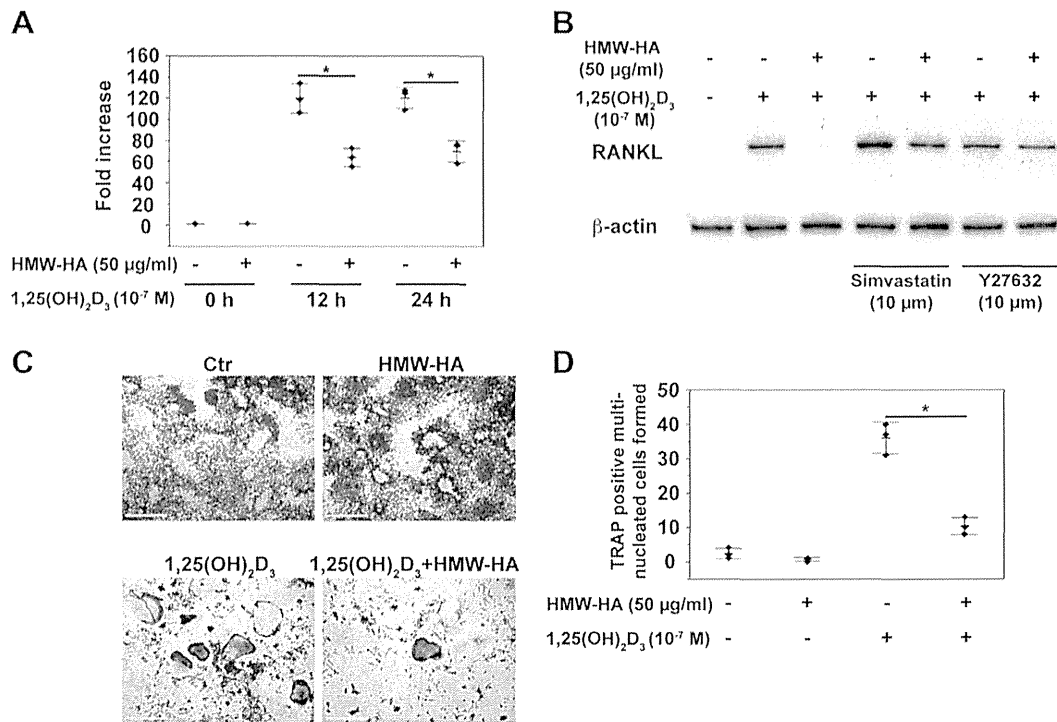
Fig. 7. Effects of HMW-HA on osteoclast formation supported by ST2 cells. (A) ST2 cells were stimulated with 1,25(OH)$_2$D$_3$ ($10^{-7}$ M) in the presence or absence of HMW-HA (50 µg/ml) for the indicated times. Total RNA was isolated and reverse transcribed into cDNA, then PCR amplification was performed using primers specific for *Rankl* and *Gapdh*. Data shows the fold changes in *Rankl* mRNA copy number values from independent samples of $n = 3$, and bars represent means with the standard deviation. Data were analyzed by Tukey's post-test after one-way ANOVA ($P < 0.0001$). The asterisk indicates $P < 0.0001$ in comparison to treatment with 1,25(OH)$_2$D$_3$. (B) ST2 cells were pretreated with simvastatin (10 µM) or Y27632 (10 µM) for 24 h, then incubated with 1,25(OH)$_2$D$_3$ ($10^{-7}$ M) in the presence or absence of HMW-HA (50 µg/ml) for 48 h. Whole cell lysates were subjected to SDS-PAGE and western blotting analyses, with the blots probed for RANKL. Equivalent protein aliquots of cell lysates were also analyzed for β-actin. (C) ST2 cells were pre-treated with 1,25(OH)$_2$D$_3$ ($10^{-7}$ M) in the presence or absence of HMW-HA (50 µg/ml) for 24 h, then co-cultured with RAW 264.7 cells for 6 days and stained for TRAP activity. Bars indicate 500 µm. (D) The number of osteoclast-like cells was counted after the staining for TRAP activity. Data shows the number of osteoclast-like cells from independent samples of $n = 3$, and bars represent means with the standard deviation. Data were analyzed by Tukey's post-test after one-way ANOVA ($P < 0.0001$). The asterisk indicates $P < 0.0001$ in comparison to treatment with 1,25(OH)$_2$D$_3$.

resorption *in vitro*[35], while inhibition of osteoclastic activity by bisphosphonate was found to prevent bone and cartilage resorption in a rat degenerative joint disease model[36]. Therefore, there is great interest in identifying the effects of HMW-HA on osteoclastogenesis as a target for developing therapeutic agents to prevent joint destruction in OA.

In the present study, we used a homogeneous clonal population of mouse bone marrow stromal ST2 cells to elucidate the effects of HMW-HA on induction of osteoclast differentiation. This cell line is known to highly express RANKL in the presence of 1,25(OH)$_2$D$_3$ and RANKL-expressing cells support the differentiation of splenic cells into osteoclasts[37]. The main advantage of the present system is that it does not contain any pre-osteoclast cells, which may also be targets of HMW-HA activities.

As shown in Figs. 1 and 3, RANKL mRNA and protein were decreased by addition of HMW-HA, indicating that it has protective effects against osteoclastogenesis. Chang et al. reported that HMW-HA (1,300 kDa) decreased osteoclast formation by bone marrow-derived macrophages and human peripheral blood monocytic cells, but not by RAW 264.7 cells[25]. In the study, they discussed that the difference in effects of HMM-HA between RAW 264.7 cells and primary osteoclast precursors may be ascribed to the independence of RAW 264.7 cells on macrophage colony stimulating factor (M-CSF) for proliferation and osteoclastic differentiation. Furthermore, our results would suggest that suppression of osteoclastogenesis by HMW-HA is also dependent on down-regulation of RANKL expression in osteoblasts/stromal cells. In contrast to those findings, Cao et al. reported that HMW-HA stimulated RANKL expression in bone marrow stromal cells[38]. We have no ready explanation

for these contrasting results, though it is possible that they reflect differences in the cell species tested or variations in culture conditions, including the presence or absence of serum.

The modified coumarin, 4-MU has been reported to specifically inhibit HA synthesis and pericellular HA matrix formation in cultured mammalian cells[29,30]. Several studies have reported the various biological effects of 4-MU on inflammatory response in arthritis[39], tumourigenicity[40], and nerve injury[41]. As shown in Figs. 2 and 3, we found that 4-MU up-regulated RANKL expression, and our observations suggest that inhibition of HA synthesis and loss of cell–matrix interaction enhance osteoclast differentiation and bone resorption. In addition, the effect of 4-MU on proliferation of ST2 cells was examined using a WST-1 assay, though no effect on cell growth up to 48 h was seen.

Another important finding of our study is that the HA receptor CD44 is required for down-regulation of RANKL mediated by HMW-HA. CD44 is one of the major HA binding proteins and expressed in several types of cells, including osteoblasts[42], while binding of HA to CD44 is known to be involved in onset of a variety of biological activities. The monoclonal rat anti-CD44 antibody recognizes a determinant of the HA binding region common to CD44 and its principal variant isoforms[43] and that antibody is routinely used in HA-related blocking experiments. As shown in [Fig. 4(A)], pre-treatment with that CD44 function-blocking monoclonal antibody resulted in significantly reduced accumulation of exogenous HMW-HA in ST2 cells. We also found that this antibody remarkably inhibited the effect of HMW-HA on down-regulation of RANKL in ST2 cells [Fig. 4(B) and (C)]. On the basis of these findings, we speculate that expression of CD44 in

ST2 cells, which have the same lineage as osteoblasts, leads to regulation of osteoclast formation and activation mediated by HMW-HA.

Rho GTPases (RhoA, Rac1, Cdc42) are members of the Rho subclass of the Ras superfamily[44], and have a cycle between active GTP-bound states and inactivate GDP-bound states in response to external stimuli. In their active form, they regulate key signaling pathways and control a variety of cellular activities, including gene transcription, cytoskeleton reorganization, cell growth, migration, and oncogenesis[45]. Previous studies have also found that HA-CD44 binding induces RhoA signaling in head and neck tumor cells[46]. In the present study, addition of HMW-HA led to a significant increase in the level of active GTP-bound RhoA [Fig. 5(A)], while pre-treatment with the CD44 function-blocking monoclonal antibody remarkably inhibited HMW-HA-induced RhoA activation in ST2 cells [Fig. 5(B)]. These results demonstrated that HA-CD44 interaction also induces RhoA signaling in osteoblasts/stromal cells.

Recent findings indicate that the RhoA signaling pathway has important roles in bone remodeling. For example, in osteoblast survival[31], the integrity of the actin cytoskeleton[32], as well as migration and differentiation[33] are regulated by RhoA signaling. Simvastatin has been reported to reduce the synthesis of mevalonate by inhibiting hydroxymethylglutaryl (HMG)-CoA reductase, finally leading to blockade of Rho GTPases by the effector proteins ROCK[47]. On the other hand, Y-27632, a pyridine derivative, was discovered to particularly disrupt ROCK signaling[48] and has been widely investigated in various studies. We found that blockage the RhoA/ROCK pathway by either simvastatin or Y-27632 prevented a decrease in RANKL expression caused by exposure to HMW-HA [Fig. 6]. These findings are consistent with a previous study, in which the expression of constitutively active RhoA in osteoblastic cells was shown to impair their ability to induce osteoclastogenesis via suppression of RANKL mRNA in response to parathyroid hormone or calcitol.[49]

As a catabolic effect on bone, $1\alpha,25(OH)_2D_3$ promotes osteoclastogenesis by up-regulating the expression of RANKL. In the present study, administration of HMW-HA decreased RANKL expression induced by $1\alpha,25(OH)_2D_3$ [Fig. 7(A)], while simvastatin and Y-27632 recovered that decreased expression in cells treated with HMW-HA [Fig. 7(B)]. HMW-HA also prevented osteoclast differentiation of co-cultured precursors supported by stromal cells expressing RANKL [Fig. 7(C) and (D)]. These results suggest that activation of RhoA/Rho kinase signaling by HMW-HA inhibits RANKL in bone marrow stromal cells, thereby inhibiting osteoclastogenesis. Furthermore, $1\alpha,25(OH)_2D_3$ was reported to suppress the gene expression of osteoprotegerin (OPG), which acts as a decoy receptor for RANKL and prevents RANK–RANKL interaction, and thus osteoclastogenesis[50]. In our study, HMW-HA recovered up-regulation of RANKL expression, while the down-regulation of OPG was mediated by $1\alpha,25(OH)_2D_3$ (data not shown). Bone resorption is a multistep process initiated by the proliferation of immature osteoclast precursors, which is followed by the commitment of those cells to the osteoclast phenotype and degradation of the organic and inorganic phases of bone by mature resorptive cells. We previously reported that TRAP positive multinucleated cells differentiated from RAW 264.7 cells by RANKL are capable of bone resorption using calcium phosphate substrate coated slides[26]. From those results, the molecular mechanism for the effect of HMW-HA on OPG expression and on osteoclast function are currently under investigation in our laboratory.

HA is known to be associated with several cell surface molecules, such as CD44, receptor for hyaluronan-mediated motility (RHAMM), toll-like receptor-4 (TLR4), and intercellular adhesion molecule (ICAM-1). It has also been reported that RHAMM, TLR4, and ICAM-1 are expressed in osteoblast stromal lineage cells. Further study is needed to examine the correlations between HMW-HA and other receptors regarding inhibition of osteoclast formation, as well as signal transduction during osteoclastogenesis.

In conclusion, the present findings showed that HMW-HA inhibits the transcription of RANKL in stromal cells by activating the RhoA/Rho kinase pathways. CD44-mediated signaling supports this activation and is likely critical for certain cell types, such as stromal cells. Furthermore, our results suggest that stromal cells have a capacity to sense changes in cell surface HA-CD44 interactions, resulting in regulation of bone metabolism. Whether analogous effect of HMW-HA on osteoclast occurs in human cells or *in vivo* animal model remains to be determined. Nonetheless, we consider that these results provide a basis to understand why HMW-HA is effective when used as treatment for OA.

## Author contributions

All of the authors were involved in drafting the article or critically revising it for important intellectual content, and all approved the final version to be published. Dr. T. Nishihara had full access to all of the data in the study, and takes responsibility for its integrity and the accuracy of the data analysis.

Study conception and design: Ariyoshi W, Okinaga T, Nishihara T.

Acquisition of data: Ariyoshi W, Knudson C.B, Knudson W, Nishihara T.

Analysis and interpretation of data: Ariyoshi W, Okinaga T, Nishihara T.

## Conflicts of interest
The authors have no conflicts of interest to disclose.

## Acknowledgments

## References

1. Lee JY, Spicer AP. Hyaluronan: a multifunctional, megaDalton, stealth molecule. Curr Opin Cell Biol 2000;12:581–6.
2. Noble PW. Hyaluronan and its catabolic products in tissue injury and repair. Matrix Biol 2002;21:25–9.
3. Goldberg VM, Buckwalter JA. Hyaluronans in the treatment of osteoarthritis of the knee: evidence for disease-modifying activity. Osteoarthritis Cartilage 2005;13:216–24.
4. Amiel D, Toyoguchi T, Kobayashi K, Bowden K, Amiel ME, Healey RM. Long-term effect of sodium hyaluronate (Hyalgan) on osteoarthritis progression in a rabbit model. Osteoarthritis Cartilage 2003;11:636–43.
5. Abatangelo G, Botti P, Del Bue M, Gei G, Samson JC, Cortivo R, et al. Intraarticular sodium hyaluronate injections in the Pond-Nuki experimental model of osteoarthritis in dogs. I. Biochemical results. Clin Orthop Relat Res 1989;241:278–85.
6. Altman RD, Moskowitz R. Intraarticular sodium hyaluronate (Hyalgan) in the treatment of patients with osteoarthritis of the knee: a randomized clinical trial. Hyalgan Study Group. J Rheumatol 1998;25:2203–12.
7. Kolarz G, Kotz R, Hochmayer I. Long-term benefits and repeated treatment cycles of intra-articular sodium hyaluronate (Hyalgan) in patients with osteoarthritis of the knee. Semin Arthritis Rheum 2003;32:310–9.
8. Knudson W, Aguiar DJ, Hua Q, Knudson CB. CD44-anchored hyaluronan-rich pericellular matrices: an ultrastructural and biochemical analysis. Exp Cell Res 1996;228:216–28.

9. Assimakopoulos D, Kolettas E, Patrikakos G, Evangelou A. Histol Histopathol 2002;17:1269–81.

10. Bourguignon LY, Singleton PA, Zhu H, Diedrich F. Hyaluronan-mediated CD44 interaction with RhoGEF and Rho kinase promotes Grb2-associated binder-1 phosphorylation and phosphatidylinositol 3-kinase signaling leading to cytokine (macrophage-colony stimulating factor) production and breast tumor progression. J Biol Chem 2003;278: 29420–34.

11. Bourguignon LY, Zhu H, Shao L, Chen YW. CD44 interaction with tiam1 promotes Rac1 signaling and hyaluronic acid-mediated breast tumor cell migration. J Biol Chem 2000;275: 1829–38.

12. Bourguignon LY, Zhu H, Zhou B, Diedrich F, Singleton PA, Hung MC. Hyaluronan promotes CD44v3-Vav2 interaction with Grb2-p185(HER2) and induces Rac1 and Ras signaling during ovarian tumor cell migration and growth. J Biol Chem 2001;276:48679–92.

13. Bourguignon LY, Zhu H, Shao L, Chen YW. CD44 interaction with c-Src kinase promotes cortactin-mediated cytoskeleton function and hyaluronic acid-dependent ovarian tumor cell migration. J Biol Chem 2001;276:7327–36.

14. Bourguignon LY, Singleton PA, Zhu H, Zhou B. Hyaluronan promotes signaling interaction between CD44 and the transforming growth factor beta receptor I in metastatic breast tumor cells. J Biol Chem 2002;277:39703–12.

15. Kohda D, Morton CJ, Parkar AA, Hatanaka H, Inagaki FM, Campbell ID, et al. Solution structure of the link module: a hyaluronan-binding domain involved in extracellular matrix stability and cell migration. Cell 1996;86:767–75.

16. Suda T, Takahashi N, Martin TJ. Modulation of osteoclast differentiation. Endocr 1992;13:66–80.

17. Suda T, Takahashi N, Udagawa N, Jimi E, Gillespie MT, Martin TJ. Modulation of osteoclast differentiation and function by the new members of the tumor necrosis factor receptor and ligand families. Endocr Rev 1999;20:345–57.

18. Darnay BG, Haridas V, Ni J, Moore PA, Aggarwal BB. Characterization of the intracellular domain of receptor activator of NF-κB (RANK): interaction with tumor necrosis factor receptor-associated factors and activation of NF-κB and c-Jun N-terminal kinase. J Biol Chem 1998;273:20551–5.

19. Fioravanti A, Cantarini L, Chellini F, Manca D, Paccagnini E, Marcolongo R, et al. Effect of hyaluronic acid (MW 500-730 kDa) on proteoglycan and nitric oxide production in human osteoarthritic chondrocyte cultures exposed to hydrostatic pressure. Osteoarthritis Cartilage 2005;13:688–96.

20. Tanaka M, Masuko-Hongo K, Kato T, Nishioka K, Nakamura H. Suppressive effects of hyaluronan on MMP-1 and RANTES production from chondrocytes. Rheumatol Int 2006;26:185–90.

21. Wang CT, Lin YT, Chiang BL, Lin YH, Hou SM. High molecular weight hyaluronic acid down-regulates the gene expression of osteoarthritis-associated cytokines and enzymes in fibroblast-like synoviocytes from patients with early osteoarthritis. Osteoarthritis Cartilage 2006;14:1237–47.

22. Cake MA, Smith MM, Young AA, Smith SM, Ghosh P, Read RA. Synovial pathology in an ovine model of osteoarthritis: effect of intraarticular hyaluronan (Hyalgan). Clin Exp Rheumatol 2008;26:561–7.

23. Lajeunesse D, Delalandre A, Martel-Pelletier J, Pelletier JP. Hyaluronic acid reverses the abnormal synthetic activity of human osteoarthritic subchondral bone osteoblasts. Bone 2003;33:703–10.

24. Pivetta E, Scapolan M, Wassermann B, Steffan A, Colombatti A, Spessotto P. Blood-derived human osteoclast resorption activity is impaired by Hyaluronan-CD44 engagement via a p38-dependent mechanism. J Cell Phyiol 2011;226:763–9.

25. Chang EJ, Kim HJ, Ha J, Kim HJ, Ryu J, Park KH, et al. Hyaluronan inhibits osteoclast differentiation via toll-like receptor 4. J Cell Sci 2007;120:166–76.

26. Ariyoshi W, Takahashi T, Kanno T, Ichimiya H, Takano H, Koseki T, et al. Mechanisms involved in enhancement of osteoclast formation and function by low molecular weight hyaluronic acid. J Biol Chem 2005;280:18967–72.

27. Rasmussen TB, Uttenthal A, de Stricker K, Belak S, Storgaard T. Development of a novel quantitative real-time RT-PCR assay for the simultaneous detection of all serotypes of foot-and-mouth disease virus. Arch Virol 2003;148:2005–21.

28. Pfaffl MW. A new mathematical model for relative quantification in real-time RT-PCR. Nucleic Acids Res 2001;29:e45.

29. Kudo D, Kon A, Yoshihara S, Kakizaki I, Sasaki M, Endo M, et al. Effect of a hyaluronan synthase suppressor, 4-methylumbelliferone, on B16F-10 melanoma cell adhesion and locomotion. Biochem Biophys Res Commun 2004;321: 783–7.

30. Nakazawa H, Yoshihara S, Kudo D, Morohashi H, Kakizaki I, Kon A, et al. 4-methylumbelliferone, a hyaluronan synthase suppressor, enhances the anticancer activity of gemcitabine in human pancreatic cancer cells. Cancer Chemother Pharmacol 2006;57:165–70.

31. Yoshida T, Clark MF, Stern PH. The small GTPase RhoA is crucial for MC3T3-E1 osteoblastic cell survival. J Cell Biochem 2009;106:896–902.

32. Kazmers NH, Ma SA, Yoshida T, Stern PH. Rho GTPase signaling and PTH 3-34, but not PTH 1-34, maintain the actin cytoskeleton and antagonize bisphosphonate effects in mouse osteoblastic MC3T3-E1 cells. Bone 2009;45:52–60.

33. Yang S, Tian YS, Lee YJ, Yu FH, Kim HM. Mechanisms by which the inhibition of specific intracellular signaling pathways increase osteoblast proliferation on apatite surfaces. Biomaterials 2011;32:2851–61.

34. Bettica P, Cline G, Hart DJ, Meyer J, Spector TD. Evidence for increased bone resorption in patients with progressive knee osteoarthritis: longitudinal results from the Chingford study. Arhthritis Rheum 2002;46:3178–84.

35. Durand M, Komarova SV, Bhargava A, Trebec-Reynolds DP, Li K, Fiorino C, et al. Monocytes from patients with osteoarthritis display increased osteoclastogenesis and bone resorption: the In vitro Osteoclast Differentiation in Arthritis study. Arthritis Rheum 2013;65:148–58.

36. Strassle BW, Mark L, Leventhal L, Piesla MJ, Jian Li X, Kennedy JD, et al. Inhibition of osteoclasts prevents cartilage loss and pain in a rat model of degenerative joint disease. Osteoarthritis Cartilage 2010;18:1319–28.

37. Udagawa N, Takahashi N, Akatsu T, Sasaki T, Yamaguchi A, Kodama H, et al. The bone marrow-derived stromal cell lines MC3T3-G2/PA6 and ST2 support osteoclast-like cell differentiation in cocultures with mouse spleen cells. Endocrinology 1989;125:1805–13.

38. Cao JJ, Singleton PA, Majumdar S, Boudignon B, Burghardt A, Kurimoto P, et al. Hyaluronan increases RANKL expression in bone marrow stromal cells through CD44. J Bone Miner Res 2005;21:30–40.

39. Yoshioka Y, Kozawa E, Urakawa H, Arai E, Futamura N, Zhuo L, et al. Suppression of hyaluronan synthesis alleviates inflammatory response in murine arthritis and in human rheumatoid synovial fibroblasts. Arthritis Rheum 2013;65: 1160–70.

40. Arai E, Nishida Y, Wasa J, Urakawa H, Zhuo L, Kimata K, et al. Inhibition of hyaluronan retention by 4-methylumbelliferone

suppresses osteosarcoma cells in vitro and lung metastasis in vivo. Br J Cancer 2011;105:1839–49.

41. Yong N, Guoping C. Upregulation of matrix metalloproteinase-9 dependent on hyaluronan synthesis after sciatic nerve injury. Neurosci Lett 2008;444:259–63.

42. García-Martínez O, Reyes-Botella C, Aguilera-Castillo O, Vallecillo-Capilla MF, Ruiz C. Antigenic profile of osteoblasts present in human bone tissue sections. Biosci Rep 2006;26:39–43.

43. Bourguignon LY, Singleton PA, Diedrich F, Stern R, Gilad E. CD44 interaction with $Na^+$-$H^+$ exchanger (NHE1) creates acidic microenvironments leading to hyaluronidase-2 and cathepsin B activation and breast tumor cell invasion. J Biol Chem 2004;279:26991–7007.

44. Hall A. Rho GTPases and the actin cytoskeleton. Science 1998;279:509–14.

45. Li X, Lim B. Rho GTPases and their role in cancer. Oncol Res 2003;13:323–31.

46. Bourguignon LY, Gilad E, Brightman A, Diedrich F, Singleton P. Hyaluronan-CD44 interaction with leukemia-associated Rho-GEF and epidermal growth factor receptor promotes Rho/Ras co-activation, phospholipase $C\varepsilon$-$Ca^{2+}$ signaling, and cytoskeleton modification in head and neck squamous cell carcinoma cells. J Biol Chem 2006;281:14026–40.

47. Fromigue O, Hay E, Modrowski D, Bouvet S, Jacquel A, Auberger P, et al. RhoA GTPase inactivation by statins induces osteosarcoma cell apoptosis by inhibiting p42/p44-MAPKs-Bcl-2 signaling independently of BMP-2 and cell differentiation. Cell Death Differ 2006;13:1845–56.

48. Uehata M, Ishizaki T, Satoh H, Ono T, Kawahara T, Morishita T, et al. Calcium sensitization of smooth muscle mediated by a Rho-associated protein kinase in hypertension. Nature 1997;389:990–4.

49. Wang J, Stern PH. Osteoclastogenic activity and RANKL expression are inhibited in osteoblastic cells expressing constitutively active Gα(12) or constitutively active RhoA. J Cell Biochem 2010;111:1531–6.

50. Kondo T, Kitazawa R, Maeda S, Kitazawa S. 1 alpha,25 dihydroxyvitamin D3 rapidly regulates the mouse osteoprotegerin gene through dual pathways. J Bone Miner Res 2004;19:1411–9.

91

# The Dectin 1 Agonist Curdlan Regulates Osteoclastogenesis by Inhibiting Nuclear Factor of Activated T cells Cytoplasmic 1 (NFATc1) through Syk Kinase

Toru Yamasaki[‡§], Wataru Ariyoshi[‡1], Toshinori Okinaga[‡], Yoshiyuki Adachi[¶], Ryuji Hosokawa[§], Shinichi Mochizuki[‖], Kazuo Sakurai[‖], and Tatsuji Nishihara[‡]

From the [‡]Division of Infections and Molecular Biology, Department of Health Promotion, [§]Division of Oral Reconstruction and Rehabilitation, Department of Oral Functions, Kyushu Dental University, Kitakyushu, Fukuoka 803-8580, Japan, the [¶]Laboratory for Immunopharmacology of Microbial Products, School of Pharmacy, Tokyo University of Pharmacy and Life Sciences, Hachioji, Tokyo 192-0392, Japan, and the [‖]Department of Chemistry and Biochemistry, The University of Kitakyushu, Kitakyushu, Fukuoka 808-0135, Japan

**Background:** Dectin 1 is found on myeloid lineage cells and contains an immunoreceptor tyrosine-based activation motif from which signals are associated with bone homeostasis.
**Results:** The dectin 1 agonist curdlan suppresses osteoclastogenesis induced by receptor activator of NF-κB ligand (RANKL).
**Conclusion:** Curdlan regulates RANKL-induced osteoclastogenesis.
**Significance:** Curdlan could be a potential therapeutic candidate in treating osteoclast-related diseases.

Several immune system cell surface receptors are reported to be associated with osteoclastogenesis. Dectin 1, a lectin receptor for β-glucan, is found predominantly on cells of the myeloid lineage. In this study, we examined the effect of the dectin 1 agonist curdlan on osteoclastogenesis. In mouse bone marrow cells and dectin 1-overexpressing RAW 264.7 cells (d-RAWs), curdlan suppressed receptor activator of NF-κB ligand (RANKL)-induced osteoclast differentiation, bone resorption, and actin ring formation in a dose-dependent manner. This was achieved within non-growth inhibitory concentrations at the early stage. Conversely, curdlan had no effect on macrophage colony-stimulating factor-induced differentiation. Furthermore, curdlan inhibited RANKL-induced nuclear factor of activated T cell cytoplasmic 1 (NFATc1) expression, thereby decreasing osteoclastogenesis-related marker gene expression, including tartrate-resistant acid phosphatase, osteoclast stimulatory transmembrane protein, cathepsin K, and matrix metallopeptidase 9. Curdlan inhibited RANKL-induced c-fos expression, followed by suppression of NFATc1 autoamplification, without significantly affecting the NF-κB signaling pathway. We also observed that curdlan treatment decreased Syk protein in d-RAWs. Inhibition of the dectin 1-Syk kinase pathway by Syk-specific siRNA or chemical inhibitors suppressed osteoclast formation and NFATc1 expression stimulated by RANKL. In conclusion, our results demonstrate that curdlan potentially inhibits osteoclast differentiation, especially NFATc1 expression, and that Syk kinase plays a crucial role in the transcriptional pathways. This suggests that the activation of dectin 1-Syk kinase interaction critically regulates the genes required for osteoclastogenesis.

Osteoclasts originate from hematopoietic precursors of the monocyte/macrophage lineage, which differentiate into multi-nucleated, giant cells specialized to resorb bone by fusion of mononuclear progenitors (1). Osteoclasts are unique in their ability to resorb bone and play an important role in regulating bone remodeling. Osteoclast precursors interact with osteoblasts and stromal cells to permit their differentiation into mature osteoclasts (2). Furthermore, osteoclast formation is induced in the presence of receptor activator of NF-κB ligand (RANKL),[2] a member of the TNF superfamily expressed by osteoblasts and bone stromal cells. RANKL interacts with the osteoclast cell surface receptor RANK, which, in turn, recruits cytosolic TNF receptor-associated factors (3), prior to activation of downstream signaling pathways. These signaling pathways include ERK, p38 MAPK, NF-κB, and activator protein 1 (AP-1), c-jun, and c-fos. Finally, expression of the nuclear factor of activated T cell cytoplasmic 1 (NFATc1), a key molecule for osteoclastogenesis, is induced (4).

Pattern recognition receptors recognize molecular signatures of microbes and play an important role in initiation of immune responses to infection (5). Dectin 1 is a type II membrane receptor containing a single extracellular, C-type, lectin-like domain (6) and an immunoreceptor tyrosine-based activation motif (ITAM) in the cytoplasmic tail (7). Dectin 1 is found on cells of the myeloid lineage, including monocytes, macrophages, neutrophils, dendritic cells, and a subset of T cells in mice (8). It has been shown that dectin 1 is a major receptor for the recognition of β-1,3-linked and/or β-1,6-linked glucans (β-glucans) (8, 9).

Dectin 1 is known to mediate its own signaling through its cytoplasmic tail (10), and tyrosine residues within its receptor

---

[1] To whom correspondence should be addressed: Div. of Infections and Molecular Biology, Dept. of Health Promotion, Kyushu Dental University, 2-6-1 Manazuru, Kokurakita-ku, Kitakyushu, Fukuoka, Japan. Tel.: 81-93-285-3051; Fax: 81-93-581-4984; E-mail: arikichi@kyu-dent.ac.jp.

[2] The abbreviations used are: RANKL, receptor activator of NF-κB ligand; ITAM, immunoreceptor tyrosine-based activation motif; BMC, bone marrow cell; α-MEM, α-minimal essential medium; M-CSF, macrophage colony-stimulating factor; ANOVA, analysis of variance; TRAP, tartrate-resistant acid phosphatase; SUMO, small ubiquitin-like modifier.

ITAM motif are phosphorylated by Src family tyrosine kinases through engagement with dectin 1. This is followed by recruitment and activation of Syk, a nonreceptor tyrosine kinase (11–13), with activation of several intracellular signaling pathways, including NF-$\kappa$B, MAPK, and NFAT (14).

The $\beta$-glucans, consisting of a backbone of polymerized $\beta$-(1,3)-linked $\beta$-D-glucopyranosyl units and $\beta$-(1,6)-linked side chains, are a major cell component of fungi and are also found in plants and some bacteria (15). They are known to possess anti-infection and antitumorigenic properties by possessing the ability to activate leukocytes by stimulating their phagocytic activity and the production of reactive oxygen intermediates and inflammatory mediators, including TNF-$\alpha$ (16–19). However, the mechanism of $\beta$-glucan-induced activity has not been elucidated precisely because pathogen-derived components are often contaminated by $\beta$-glucan preparations. Recently, curdlan, a linear nonionic homopolymer of D-glucose with 1,3 glucosidic linkages, has been identified as a dectin 1-specific agonist and has gained attention from the pharmaceutical industry as an immunomodulatory drug delivery vehicle (20, 21).

Several cell surface receptors in the immune system are reported to be associated with osteoclastogenesis. ITAM-dependent costimulatory signals, activated by multiple immunoreceptors, are essential for the maintenance of bone homeostasis (22). It has been demonstrated that Syk modulates osteoclast function *in vitro* and *in vivo* (23–25). However, the direct effects of $\beta$-glucans on osteoclastogenesis are largely unknown. In this study, we examined the effect of curdlan, a linear homopolymer of D-glucose, on osteoclastogenesis. We also identified the precise mechanisms by which curdlan suppresses osteoclast formation *in vitro*.

## EXPERIMENTAL PROCEDURES

*Reagents and Antibodies*—Curdlan was purchased from Wako Pure Chemical Industries (Osaka, Japan) and diluted with 0.1 N NaOH. Anti-NFATc1 polyclonal antibody, anti-I$\kappa$B-$\alpha$ polyclonal antibody, and anti-RANK polyclonal antibody were obtained from Santa Cruz Biotechnology (Santa Cruz, CA), and anti-$\beta$-actin monoclonal antibody was purchased from Sigma-Aldrich (St. Louis, MO). Anti-c-fos monoclonal antibody, anti-Syk polyclonal antibody, anti-phospho-Syk monoclonal antibody, anti-c-jun monoclonal antibody, anti-phospho-c-jun monoclonal antibody, and anti-histone H3 monoclonal antibody were purchased from Cell Signaling Technology Inc. (Beverly, MA). Anti-dectin 1 polyclonal antibody was purchased from R&D Systems (Minneapolis, MN).

*Cell Culture*—Bone marrow cells (BMCs) were isolated from femurs and tibias of 6-week-old male ddY mice (Kyudo Co., Ltd., Saga, Japan) and maintained in $\alpha$-minimum essential medium ($\alpha$-MEM; Invitrogen) supplemented with 10% FCS (Sigma-Aldrich), 100 units/ml penicillin G potassium salt (Nacalai Tesque, Kyoto, Japan), and 100 $\mu$g/ml streptomycin (Wako Pure Chemical Industries). Cells ($4 \times 10^4$) were cultured with M-CSF (20 ng/ml, Peprotech, Rocky Hill, NJ) and RANKL (40 ng/ml, Peprotech) in the presence or absence of curdlan on 48-well plates at 37 °C in 5% $CO_2$ for 4 days to generate mature osteoclasts. All procedures were approved by the Animal Care and Use Committee of Kyushu Dental University.

To prepare the dectin 1 retrovirus vector, cDNA-encoded mouse dectin 1 was cloned into the pFB-Neo plasmid (Agilent Technologies, Inc., Santa Clara, CA). GP2-293 packaging cells (Clontech Laboratories, Inc., Mountain View, CA) were transfected by a plasmid mixture containing dectin 1/pFB-Neo and pVSV-G (Clontech Laboratories, Inc.) with Lipofectamine LTX (Invitrogen) in accordance with the protocol of the manufacturer. The culture supernatant of GP2-293 cells was harvested as a retrovirus fluid for dectin 1 transfection. RAW 264.7 cells (Riken Cell Bank, Tsukuba, Japan) were cultured with the virus vector in the presence of 8 $\mu$g/ml Polybrene for 48 h. Cells expressing dectin 1 (d-RAW) were maintained in $\alpha$-MEM containing 10% FCS, penicillin G (100 units/ml), streptomycin (100 $\mu$g/ml), and G418 disulfate aqueous solution (50 mg/ml, Nacalai Tesque). For the negative control of d-RAW cells, a control virus vector without dectin 1 cDNA was used for infection (c-RAW). The expression of dectin 1 molecules on RAW 264.7 cells was examined by antibody staining using anti-mouse dectin 1 (clone RH1, BioLegend, San Diego, CA). Cells ($1 \times 10^3$ cells/well) were cultured for 7 days with RANKL (40 ng/ml) in the presence or absence of curdlan on 96-well plates at 37 °C in 5% $CO_2$ to generate mature osteoclasts. In some experiments, cells were treated with selective inhibitors of Syk kinase, piceatannol (Calbiochem, San Diego, CA) and BAY 61-3606 (Calbiochem), for 1 h prior to stimulation with RANKL in the presence or absence of each inhibitor. Mouse bone marrow stromal cells, ST2, were obtained from the Riken Cell Bank and maintained in $\alpha$-MEM supplemented with 10% FCS, 100 units/ml penicillin G, and 100 mg/ml streptomycin at 37 °C in an atmosphere of 5% $CO_2$.

*Evaluation of Osteoclast Differentiation*—After culture, adherent cells were fixed and stained with TRAP using a leukocyte acid phosphatase kit (Sigma-Aldrich). TRAP-positive multinucleated cells containing three or more nuclei were considered to be osteoclasts and were counted using a microscope.

*Assessment of Actin Ring Formation*—Mature osteoclasts were prepared from BMCs by treatment with M-CSF (20 ng/ml) and RANKL (40 ng/ml) in the presence or absence of curdlan for 5 days on 8-well chamber slides (Thermo Fisher Scientific, Waltham, MA). In some experiments, d-RAWs were cultured for 8 days with RANKL (40 ng/ml) in the presence or absence of curdlan for 8 days on the chamber slides. Cells were fixed with 4% paraformaldehyde in PBS for 60 min at 4 °C, quenched with 0.2 M glycine in PBS, and permeabilized using 0.2% Triton X-100 for 10 min at room temperature. After washing in PBS, cells were incubated with Alexa Fluor 488-phalloidin (Invitrogen) for 60 min at room temperature and then washed, mounted in mounting medium containing nuclear DAPI stain (Vector Laboratories Inc., Burlingame, CA), and visualized using a BZ-9000 fluorescence microscope (Keyence Corp., Osaka, Japan). Images were captured digitally in real time and processed using BZ-II imaging software (Keyence Corp.).

*Assessment of Bone Resorption*—For the bone resorption assay, BMCs were cultured for 7 days with M-CSF (20 ng/ml) and RANKL (40 ng/ml) in the presence or absence of curdlan on an Osteo Assay Stripwell Plate® (Corning Inc., NY). d-RAWs were cultured for 10 days with RANKL (40 ng/ml) in

93
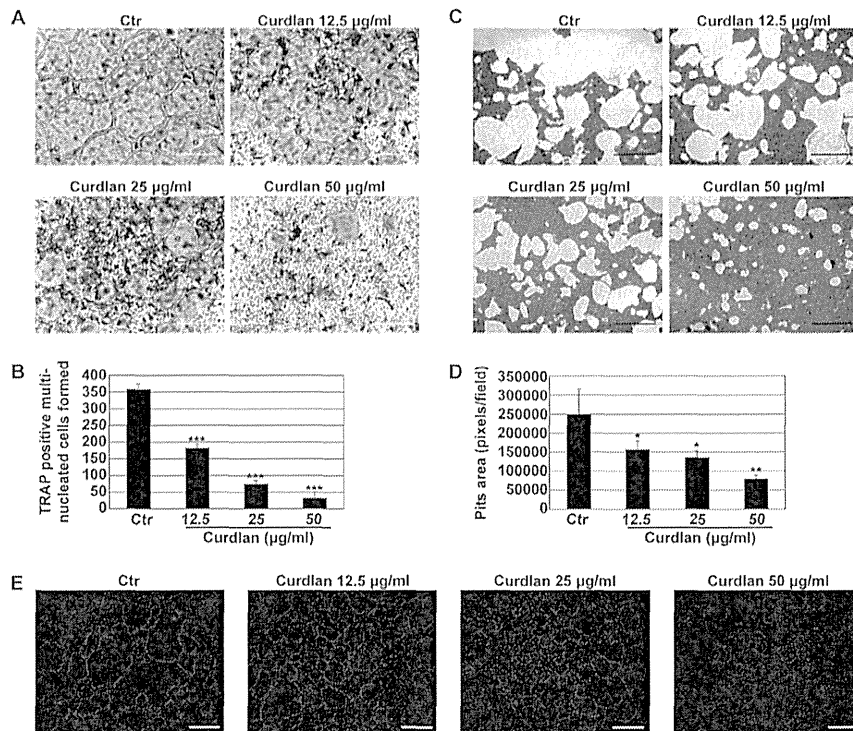
FIGURE 1. **Effect of curdlan on osteoclastogenesis in BMCs.** *A,* mouse BMCs were incubated with M-CSF (20 ng/ml) and RANKL (40 ng/ml) in the presence or absence of curdlan (12.5–50 $\mu$g/ml). Cells were cultured for 4 days and stained for TRAP activity. *Scale bars* = 500 $\mu$m. *Ctr,* control. *B,* the number of osteoclasts was counted after staining for TRAP activity. Data show the number of osteoclasts from three independent samples, and *error bars* represent mean ± S.D. Data were analyzed by Dunnett's test after one-way ANOVA. ***, $p < 0.0001$ in comparison with the control without curdlan treatment. *C,* BMCs were incubated with M-CSF (20 ng/ml) and RANKL (40 ng/ml) in the presence or absence of curdlan (12.5–50 $\mu$g/ml) on an Osteo Assay Stripwell Plate® for 7 days. Cells were removed, and the resorption pits were visualized with light microscopy. *Scale bars* = 500 $\mu$m. *D,* the pit areas were analyzed with ImageJ software. Data show the resorption area from three independent samples, and *error bars* represent mean ± S.D. Data were analyzed by Dunnett's test after one-way ANOVA. *, $p < 0.05$; **, $p < 0.01$ in comparison with the control without curdlan treatment. *E,* BMCs were incubated with M-CSF (20 ng/ml) and RANKL (40 ng/ml) in the presence or absence of curdlan (12.5–50 $\mu$g/ml) for 5 days. Cells were fixed and stained for F-actin. *Scale bars* = 500 $\mu$m.

the presence or absence of curdlan. To quantitate resorption lacunae, cells were removed with 5% sodium hypochlorite, followed by extensive washing with distilled water and air drying. In some experiments for a pit assay, BMCs were cultured with M-CSF (20 ng/ml) and RANKL (40 ng/ml) in the presence or absence of curdlan on dentin slices (Wako Pure Chemical Industries). Cells on dentin slices were removed, and pits were stained with Mayer's hematoxylin solution (Muto Pure Chemicals Co., Ltd., Tokyo, Japan). The absorbed areas on the discs and dentin slices were observed under a microscope and quantified using ImageJ software (National Institutes of Health, http://rsb.info.nih.gov).

*Quantitative Real-time RT-PCR*—Total RNA was isolated from cells with an RNeasy mini kit (Qiagen Inc., Valencia, CA) according to the instructions of the manufacturer. RNA was transcribed with q-Script cDNA Supermix reagents (Quanta BioSciences, Gaitherburg, MD) and amplified for 30 min at 42 °C. For real-time RT-PCR, PCR products were detected using FAST SYBR® Green Master Mix (Applied Biosystems, Foster City, CA) using the following primer sequences: *gapdh,* 5′-GACGGCCGCATCTTCTTGA-3′ (forward) and 5′-CAC-ACCGACCTTCACCATTTT-3′ (reverse); *dectin 1,* 5′-CCTT-GGAGGCCCATTGC-3′ (forward) and 5′-GCAACCACTAC-TACCACAAAGC A-3′ (reverse); *nfatc1,* 5′-ACCACCTTTC-CGCAA CCA-3′ (forward) and 5′-GGTACTGGCTTCTCT

TCCGTTTC-3′ (reverse); *trap,* 5′-CTGCTGGGC CTACAA-ATCATA-3′ (forward) and 5′-GGGAG TCCTCAGATCC-ATAGT-3′ (reverse); *oc-stamp,* 5′-CCGCAGCCTGACATTT-GAG-3′ (forward) and 5′-TCTCCTGAGTGATCGTGTG-CAT-3′ (reverse); *cathepsin k,* 5′-TATGACCACTGCCTTC CAATAC-3′ (forward) and 5′-GCCGTGGCGTTA TACAT-ACA-3′ (reverse); and *mmp9,* 5′-TGAGCTGG ACAGCCAG-ACACTAAA-3′ (forward) and 5′-T CGCGGCAAGTCTTCA-GAGTAGTT-3′ (reverse). Thermal cycling and fluorescence detection were performed using a StepOne™ real-time system (Applied Biosystems). Relative changes in gene expression were calculated using the comparative CT method. Total cDNA abundance between samples was normalized using primers specific to the *GAPDH* gene.

*Immunoblot Analysis*—Total protein was extracted using cell lysis buffer (Cell Signaling Technology) containing a protease inhibitor mixture (Thermo Fisher Scientific) and a phosphatase inhibitor mixture (Nacalai Tesque). Protein contents were measured using a DC protein assay kit (Bio-Rad). Total protein (20 $\mu$g/sample) was loaded and separated on a 10–20% e-PAGEL (ATTO Corp., Tokyo, Japan) and then transferred to PVDF membranes (Millipore Corp., Bedford, MA). Nonspecific binding sites were blocked for 30 min by immersing the membrane in Blocking One (Nacalai Tesque) at room temperature. Membranes were subjected to overnight incubation with

94
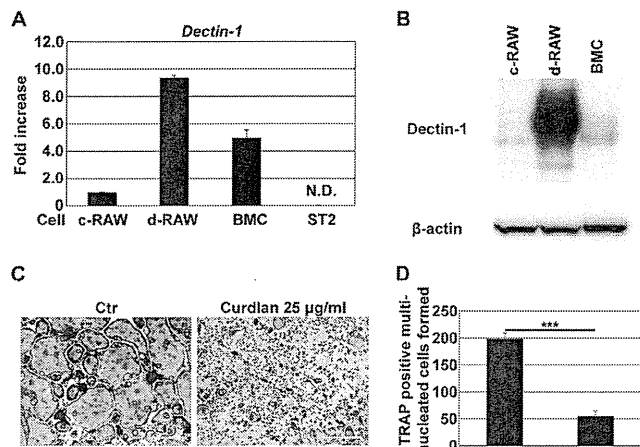
FIGURE 2. **Expression of dectin 1 in c-RAWs, d-RAWs, BMCs, and ST2 cells.** A, total RNA was isolated from c-RAWs, d-RAWs, BMCs, and ST2, reverse-transcribed into cDNA, and then PCR amplification was performed using primers specific for *dectin 1* and *Gapdh*. Data show the fold changes in *dectin 1* mRNA copy number values from three independent samples. *Error bars* represent mean ± S.D. N.D. represents not detected. B, whole cell lysates from c-RAW, d-RAW, and BMCs were subjected to SDS-PAGE and Western blotting analyses, with the blots probed for dectin 1. Equivalent protein aliquots of cell lysates were also analyzed for β-actin. C, mouse BMCs were incubated overnight on culture dishes in α-MEM containing 10% FCS. After discarding adherent cells, floating cells were incubated further with M-CSF (20 ng/ml) on Petri dishes, BMCs became adherent after a 3-day culture and were used as osteoclast precursors. Osteoclast precursors were cultured further with M-CSF + RANKL (40 ng/ml) in the presence or absence of curdlan (25 μg/ml) for 3 days. Cells were stained for TRAP activity. *Scale bars* = 500 μm. *Ctr*, control. D, the number of osteoclasts was counted after staining for TRAP activity. Data show the number of osteoclasts from three independent samples, and *error bars* represent mean ± S.D. Data were analyzed by Dunnett's test after one-way ANOVA. ***, $p < 0.0001$ in comparison with control without curdlan treatment.

diluted primary antibodies at 4 °C, followed by HRP-conjugated secondary antibodies for 60 min at room temperature. HRP-conjugated anti-mouse and anti-rabbit IgG were used as secondary antibodies (GE Healthcare, Little Chalfont, UK). After washing the membranes, chemiluminescence was produced using ECL reagent (Amersham Biosciences, Uppsala, Sweden) or Chemi-Lumi One Super (Nacalai Tesque) and detected digitally with GelDoc XR Plus (Bio-Rad).

*Nuclear Translocation of NFATc1*— d-RAWs were cultured with or without curdlan (25 μg/ml) in the presence of RANKL (40 ng/ml) for 6 h. Cultured cells were harvested and collected by centrifugation at 300 × g for 5 min, and cell pellets were treated with NE-PER nuclear and cytoplasmic extraction reagents (Thermo Scientific) according to the instructions of the manufacturer. Cell fractions were subjected to SDS-PAGE and immunoblotted with antibody against NFATc1. In other experiments, d-RAWs were cultured with or without curdlan (25 μg/ml) in the presence of RANKL (40 ng/ml) for 3 h in 8-well chamber slides. Treated cells were fixed in 4% paraformaldehyde in PBS for 60 min at 4 °C and quenched with 0.2 M glycine in PBS. Cells were permeabilized using 0.2% Triton X-100 for 10 min at room temperature, followed by blocking with 1% BSA (Sigma-Aldrich) in PBS for 30 min. After washing in PBS, cells were incubated with anti-NFATc1 (2.0 μg/ml) antibody for 60 min at room temperature. After washing in PBS, cells were incubated with Alexa Fluor 488 conjugated anti-mouse secondary antibody (Invitrogen) and then washed, mounted in mounting medium containing DAPI, and visualized using a BZ-9000 fluorescence microscope. Images were
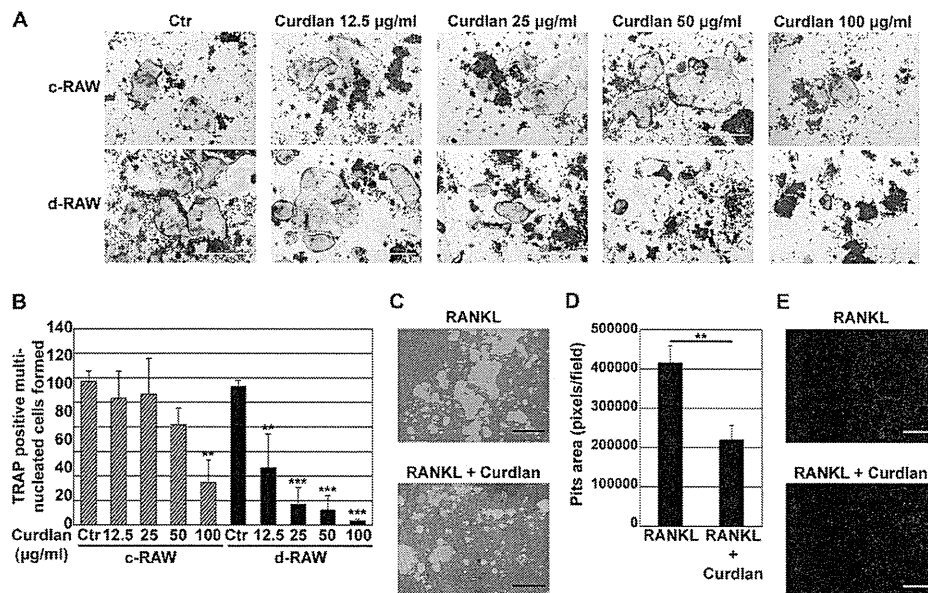
FIGURE 3. **Effect of curdlan on osteoclastogenesis in RAW 264.7 cells.** A, c-RAWs and d-RAWs were incubated with RANKL (40 ng/ml) in the presence or absence of curdlan (12.5–50 μg/ml). Cells were cultured for 7 days and stained for TRAP activity. *Scale bars* = 500 μm. *Ctr*, control. B, the number of osteoclasts was counted after staining for TRAP activity. Data show the number of osteoclasts from three independent samples, and *error bars* represent mean ± S.D. Data were analyzed by Dunnett's test after one-way ANOVA. **, $p < 0.01$; ***, $p < 0.0001$ in comparison with the control without curdlan treatment. C, d-RAWs were incubated with RANKL (40 ng/ml) in the presence or absence of curdlan (25 μg/ml) on an Osteo Assay Stripwell Plate® for 12 days. Cells were removed and the resorption pits were visualized with light microscopy. *Scale bars* = 500 μm. D, the pit areas were analyzed with ImageJ software. Data show the resorption area from three independent samples, and *error bars* represent mean ± S.D. Data were analyzed by Student's *t* test. **, $p < 0.01$ in comparison with the control without curdlan treatment. E, d-RAWs were incubated with RANKL (40 ng/ml) in the presence or absence of curdlan (25 μg/ml) for 8 days. Cells were fixed and stained for F-actin. *Scale bars* = 500 μm.

95
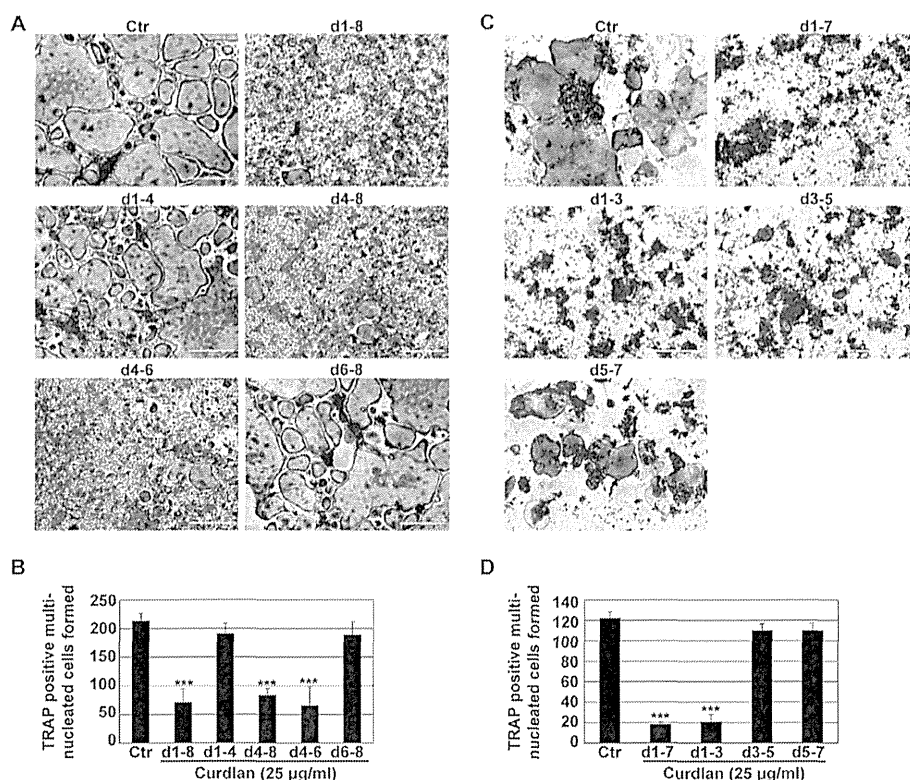
FIGURE 4. **Time course effect of curdlan on osteoclast formation in BMCs and d-RAWs.** *A*, BMCs were incubated with M-CSF (20 ng/ml) for 3 days and cultured further with M-CSF + RANKL (40 ng/ml) in the presence or absence of curdlan (25 $\mu$g/ml) for 4 days (*d*). Cells were stained for TRAP activity. *Scale bars* = 500 $\mu$m. *Ctr*, control. *C*, d-RAWs were incubated with RANKL (40 ng/ml) in the presence or absence of curdlan (25 $\mu$g/ml). Cells were cultured for 7 days and stained for TRAP activity. *Scale bars* = 500 $\mu$m. The number of osteoclasts differentiated from BMCs (*B*) and d-RAWs (*D*) was counted after the staining for TRAP activity. Data show the number of osteoclasts from three independent samples, and *error bars* represent mean ± S.D. Data were analyzed by Dunnett's test after one-way ANOVA. ***, $p < 0.0001$ in comparison with the control without curdlan treatment.

captured digitally in real time and processed using BZ-II imaging software.

*Immunofluorescence Analysis of Syk*—d-RAWs were cultured with or without curdlan (25 $\mu$g/ml) for the indicated times in 8-well chamber slides. Treated cells were fixed in 4% paraformaldehyde in PBS for 60 min at 4 °C and quenched with 0.2 M glycine in PBS. Cells were permeabilized using 0.2% Triton X-100 for 10 min at room temperature, followed by blocking with 1% BSA in PBS for 30 min. After washing in PBS, cells were incubated with anti-Syk polyclonal antibody (Santa Cruz Biotechnology, 2.0 $\mu$g/ml) overnight at 4 °C. After washing in PBS, cells were incubated with Alexa Fluor 488-conjugated anti-rabbit secondary antibody (Invitrogen) and then washed, mounted in mounting medium containing DAPI, and visualized using a BZ-9000 fluorescence microscope (Keyence Corp.). Images were captured digitally in real time and processed using BZ-II imaging software.

*Silencing of Syk Expression by Specific siRNA*—siRNA targeting was used to knock down *Syk* expression in d-RAWs. siRNA against mouse Syk and siRNA were purchased from Santa Cruz Biotechnology. A NEPA21 Super Electroporator (Nepa Gene Co., Ltd., Chiba, Japan) was used to deliver siRNA into cells according to the instructions of the manufacturer. In brief, $1.0 \times 10^6$ cells were suspended in 100 $\mu$l of $\alpha$-MEM and transfected with siRNA at a final concentration of 300 nM. Transfected cells were immediately diluted with prewarmed $\alpha$-MEM

and cultured in 6-well plates for 24 h before stimulation with RANKL. Specific gene knockdowns were assessed by real-time RT-PCR.

*Statistical Analyses*—All data were obtained from three independent experiments, and each experiment was performed in triplicate. Statistical analyses were carried out using JMP® software, version 10.0.2 (SAS Institute Inc., Cary, NC). All data were expressed as mean ± S.D. and analyzed by one-way analysis of variance (ANOVA) followed by a suitable post test (Dunnett's or Tukey's) or Student's $t$ test. $p < 0.05$ was considered to be statistically significant.

## RESULTS

*Curdlan Inhibits Osteoclast Formation and Function in BMCs*—To determine whether curdlan affects osteoclast differentiation, we first evaluated the osteoclast number by counting TRAP-positive multinucleated cells. Curdlan inhibited the differentiation of BMCs into osteoclast-like cells, mediated by M-CSF and RANKL. As shown in Fig. 1, *A* and *B*, the effect of curdlan was dose-dependent, with maximum inhibition observed at a concentration of 50 $\mu$g/ml (91.1% inhibition). Differentiated mature osteoclasts can resorb the mineral substratum on discs coated with calcium phosphate as well as dentin slices (26–28). To determine whether curdlan affects osteoclast function, differentiated BMCs were cultured on an Osteo Assay Stripwell Plate® with M-CSF and RANKL in the presence

96
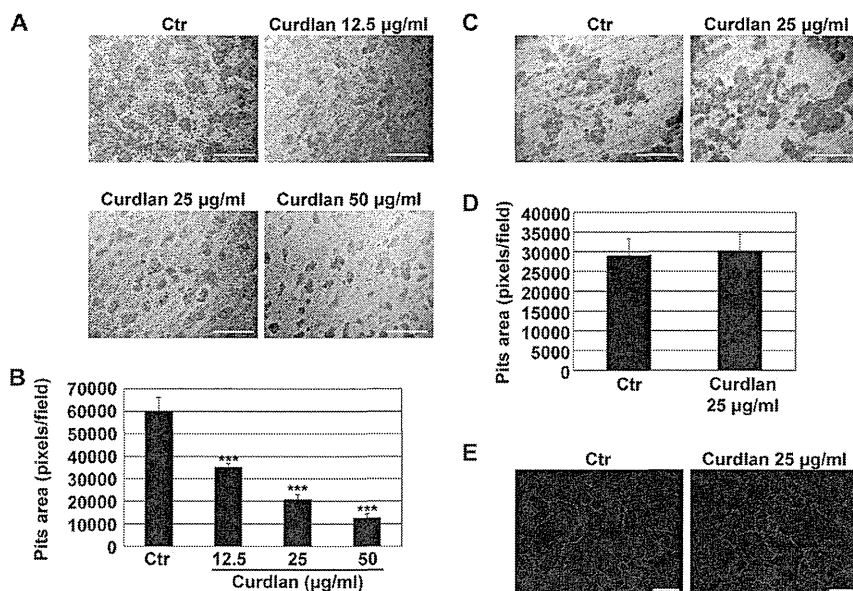
FIGURE 5. **Time course effect of curdlan on osteoclast activity in BMCs.** *A*, BMCs were incubated with M-CSF (20 ng/ml) and RANKL (40 ng/ml) in the presence or absence of curdlan (25 $\mu$g/ml) on dentin slices for 7 days. Dentin slices were stained with Mayer's hematoxylin after removal of cells. The resorption pits were visualized by light microscopy. *Scale bars* = 200 $\mu$m. *Ctr*, control. *B*, the pit areas were analyzed with ImageJ software. Data show the resorption area from three independent samples, and *error bars* represent mean ± S.D. Data were analyzed by Dunnett's test after one-way ANOVA. ***, $p < 0.001$ compared with the controls without curdlan treatment. *C*, BMCs were incubated with M-CSF (20 ng/ml) and RANKL (40 ng/ml) using RedCell® for 5 days. Mature osteoclasts were harvested and seeded on dentin slices, followed by treatment with or without curdlan (25 $\mu$g/ml) for an additional 2 days. Dentin slices were stained with Mayer's hematoxylin after removal of cells. The resorption pits were visualized by light microscopy. *Scale bars* = 200 $\mu$m. *D*, the pit areas were analyzed with ImageJ software. Data show the resorption area from three independent samples, and *error bars* represent mean ± S.D. *E*, mature osteoclasts were stimulated by curdlan (25 $\mu$g/ml) for 1 day. Cells were fixed and stained for F-actin. *Scale bars* = 500 $\mu$m.

or absence of curdlan. Curdlan inhibited the stimulatory effect of M-CSF and RANKL on bone resorption in a dose-dependent manner up to 50 $\mu$g/ml (Fig. 1, *C* and *D*). The actin sealing ring in osteoclasts is essential for bone resorption. Therefore, we visualized the actin cytoskeleton of differentiated BMCs by rhodamine-phalloidin staining. As shown in Fig. 1*E*, M-CSF and RANKL treatment induced well defined actin sealing ring formation, with a higher-intensity ring height at the cell margin. Conversely, curdlan significantly decreased the number of well defined actin rings and reduced their intensity. Curdlan had no effect on the proliferation of BMCs (data not shown).

*Curdlan-Dectin 1 Interaction Inhibits Osteoclast Formation and Function in RAW Cells*—Because the results from Fig. 1 suggested the potential relevance of curdlan in the regulation of osteoclastogenesis, we analyzed the expression of the curdlan-specific receptor dectin 1 in osteoclast precursors and stromal cells. We confirmed the expression of dectin 1 in osteoclast precursor RAW 264.7 cells and BMCs (Fig. 2, *A* and *B*). In contrast, dectin 1 gene expression was not observed in stromal ST2 cells, suggesting that the target cells of curdlan in the regulation of osteoclastogenesis are osteoclast precursors cells, not osteoblasts/stromal cells. These data were supported by the result that curdlan significantly suppressed osteoclast differentiation from osteoclast precursors derived from BMCs (Fig. 2, *C* and *D*). Therefore, the inhibitory effect of curdlan on the osteoclastogenesis of RAW 264.7 cells was evaluated *in vitro*. We found that curdlan had no effect on cell proliferation of c-RAWs and d-RAWs (data not shown). After 7 days of incubation with curdlan (12.5 $\mu$g/ml), there was a 58.8% decrease in the number of osteoclasts differentiated by RANKL in d-RAWs (Fig. 3, *A*

and *B*). This effect of curdlan was dose-dependent, with maximum inhibition observed at 100 $\mu$g/ml (97.0% inhibition). On the other hand, curdlan slightly suppressed osteoclast formation in c-RAWs, and significant inhibition was observed only at a dose of 100 $\mu$g/ml. Curdlan also inhibited RANKL-induced bone resorption (Fig. 3, *C* and *D*) and actin ring formation (Fig. 3*E*) in differentiated d-RAWs.

*Curdlan Has No Effect on M-CSF-induced BMC Differentiation but Inhibits RANKL-induced Osteoclast Formation at an Early Stage*—Osteoclastogenesis is a multistep process that can be separated into two major events: the proliferation of BMCs and their differentiation into osteoclast precursors, induced by M-CSF, and the subsequent differentiation of osteoclast precursors into osteoclasts, induced by RANKL (29). To examine which is the most important step to induce the suppressive effect of curdlan on osteoclastogenesis, we first investigated the effect of curdlan on BMC differentiation induced by M-CSF. Curdlan had almost no effect on M-CSF-induced osteoclast formation (Fig. 4, *A* and *B*, *d1-4*). To examine the precise effects of curdlan on BMC differentiation into osteoclast precursors induced by M-CSF, the expression level of an M-CSF-induced osteoclast precursor marker, RANK, was assessed by Western blotting. However, curdlan had little effect on the expression of RANK induced by M-CSF (data not shown).

To determine the effect of curdlan on RANKL-induced differentiation of osteoclast precursor cells into mature osteoclasts, we examined the differentiation process of BMCs during 8-day RANKL stimulation in the presence or absence of curdlan. We observed that stimulation of curdlan strongly inhibited RANKL-induced osteoclast differentiation during the

97

early stage (days 4–6) of differentiation. However, curdlan had no inhibitory effect on osteoclast differentiation at later stages (days 6–8). In d-RAWs, treatment with curdlan during the early stage (days 1–3) had an almost identical suppressive effect on osteoclast differentiation induced by RANKL (Fig. 4, C and D).

*Curdlan Has Little Effect on Mature Osteoclast Bone Resorption and Actin Ring Formation*—We investigated whether curdlan inhibited osteoclast bone resorption. When BMCs were cultured on dentin slices, mature osteoclasts caused the resorption of lacunae and the formation of pits in the presence of M-CSF and RANKL. The number and area of pits on the surface of the dentin slices were decreased markedly by the addition of curdlan at the beginning of the assay (Fig. 5, A and B). However, after M-CSF and RANKL stimulation for 6 days on RedCell® (CellSeed Inc., Tokyo, Japan), mature osteoclasts formed and were then seeded on dentin slices, followed by incubation in the presence or absence of curdlan for an additional 2 days. Bone resorption pits and erosion areas showed no significant differences between the control slices and curdlan-treated slices (Fig. 5, C and D). To investigate the effect of curdlan on mature osteoclasts, we examined actin ring formation. Curdlan exerted little effect on the actin ring formation of mature osteoclast (Fig. 5E).

*Curdlan Inhibits RANKL-mediated NFATc1 Expression via Dectin 1*—NFATc1 is a transcription factor essential for RANKL-stimulated osteoclastogenesis (30). Therefore, we investigated *Nfatc1* mRNA accumulation, which is related to the autoamplification of NFATc1. After 72 h of incubation with RANKL, there was a strong increase in *Nfatc1* mRNA copy number compared with untreated cells. Culturing with curdlan suppressed the stimulation of *Nfatc1* mRNA expression by RANKL in d-RAWs (Fig. 6A). In contrast, curdlan had almost no effect on expression levels of *Nfatc1* mRNA stimulated by RANKL in c-RAWs. As shown in Fig. 6B, the level of NFATc1 protein expression was increased in d-RAWs 72 h after stimulation with RANKL, and that stimulation was down-regulated by the addition of curdlan. Similar results were obtained for M-CSF and RANKL-induced NFATc1 protein expression in BMCs (Fig. 6C).

*Curdlan Negatively Regulates the Expression of Osteoclastogenic Genes*—To further substantiate the effect of curdlan on osteoclastogenesis, we examined the expression levels of mRNAs encoding osteoclast-related genes after 72 h of RANKL stimulation in d-RAWs. Consistent with the finding for osteoclastogenesis, the expression profiles revealed that osteoclast-associated genes, including *Trap* (Fig. 7A), *Oc-stamp* (Fig. 7B), *Cathepsin K* (Fig. 7C), and *Mmp9* (Fig. 7D), induced by RANKL, were decreased significantly by curdlan.

*Curdlan Inhibits the RANKL-mediated AP-1 Signaling Pathway via Dectin-1*—To investigate the molecular mechanism by which curdlan inhibits osteoclastogenesis, we evaluated the effect of curdlan on the activation of NF-κB and AP-1, which is required for induction of NFATc1, by Western blotting. RANKL induced NF-κB activation, which was observed by IκB-α degradation (Fig. 8A). Furthermore, the levels of c-jun phosphorylation (Fig. 8B, phospho-c-jun) and c-fos (Fig. 8C) expression were elevated by RANKL. When d-RAWs were
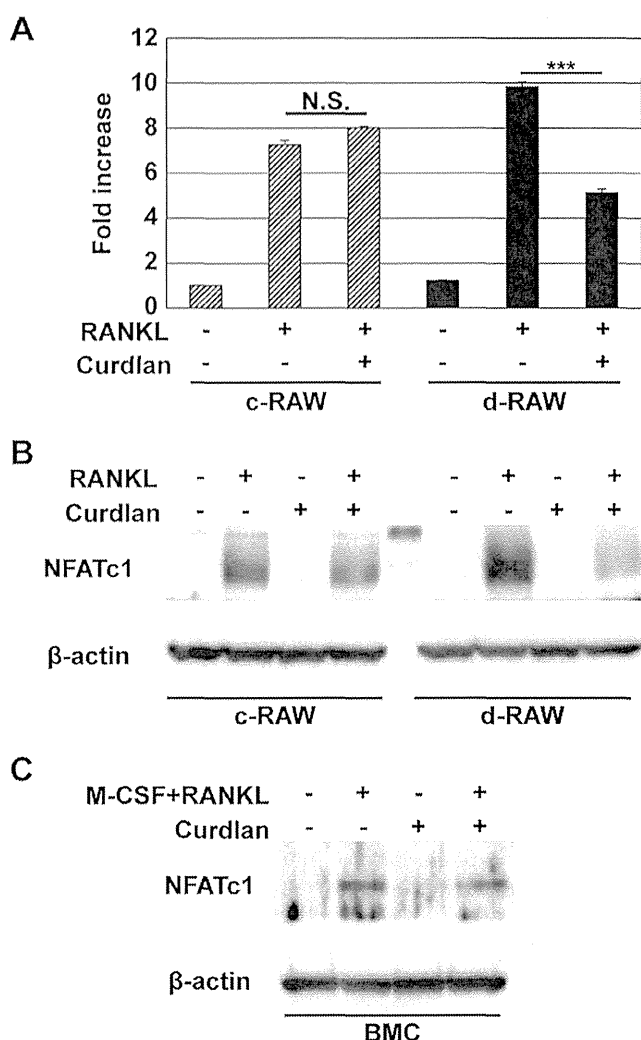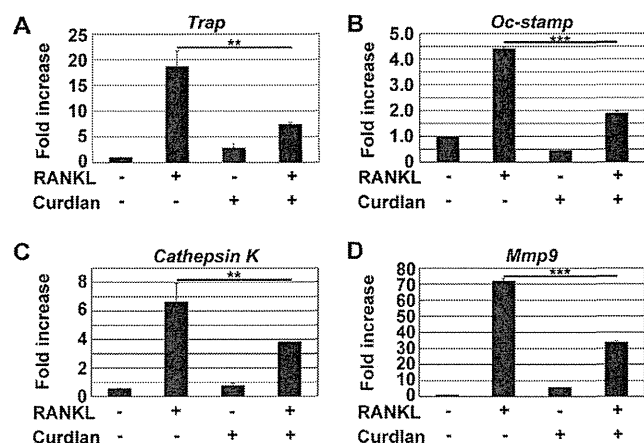


FIGURE 6. **Effect of curdlan on NFATc1 expression in RAW cells.** c-RAWs and d-RAWs were incubated with or without curdlan (25 μg/ml) in the presence of RANKL (40 ng/ml) for 72 h. A, total RNA was isolated and reverse-transcribed into cDNA, and then PCR amplification was performed using primers specific for *Nfatc1* and *Gapdh*. Data show the fold changes in *Nfatc1* mRNA copy number values from three independent samples, and *error bars* represent mean ± S.D. Data were analyzed by Tukey's post test after one-way ANOVA. ***, $p < 0.0001$ in comparison with treatment with RANKL; *N.S.*, not significant. B, whole cell lysates were subjected to SDS-PAGE and Western blot analyses, with the blots probed for NFATc1. Equivalent protein aliquots of cell lysates were also analyzed for β-actin. C, BMCs were incubated with or without curdlan (25 μg/ml) in the presence or absence of M-CSF (20 ng/ml) and RANKL (40 ng/ml) for 48 h. Whole cell lysates were subjected to SDS-PAGE and Western blot analyses, with the blots probed for NFATc1. Equivalent protein aliquots of cell lysates were also analyzed for β-actin.

incubated with RANKL and curdlan, the level of c-fos expression was lower than in cells treated with RANKL alone. This inhibitory effect of curdlan on RANKL-induced c-fos expression was not significant in c-RAWs. On the other hand, the activation of c-jun or IκB-α protein induced by RANKL was not affected by treatment with curdlan.

*Curdlan Inhibits NFATc1 Translocation to the Nucleus*—NFATc1, which is phosphorylated in the cell cytoplasm, is translocated from the cytoplasm to the nucleus by calcineurin-mediated dephosphorylation. Therefore, we investigated whether RANKL-induced NFATc1 translocation is suppressed
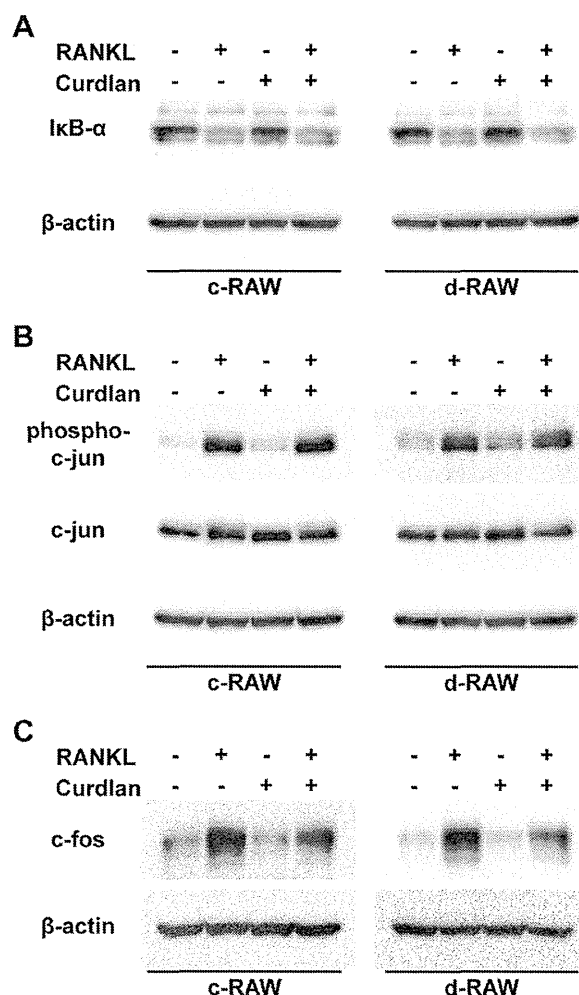
FIGURE 7. **Effect of curdlan on RANKL-induced expression of osteoclastogenic genes in d-RAWs.** d-RAWs were incubated with or without curdlan (25 $\mu$g/ml) in the presence of RANKL (40 ng/ml) for 72 h. Total RNA was isolated and reverse-transcribed into cDNA, and then PCR amplification was performed using primers specific for *Trap, Oc-stamp, Cathepsin K, Mmp9,* and *Gapdh.* Data show the fold changes in *Trap* (*A*), *Oc-stamp* (*B*), *Cathepsin K* (*C*), and *Mmp9* (*D*) mRNA copy number values from three independent samples, and *error bars* represent mean ± S.D. Data were analyzed by Tukey's post test after one-way ANOVA. \*\*, $p < 0.01$; \*\*\*, $p < 0.0001$ in comparison with treatment with RANKL.

by curdlan treatment. Nuclear translocation of NFATc1 was detected in d-RAWs treated with RANKL and was observed to be down-regulated by the addition of curdlan. (Fig. 9, *A* and *B*). Western blotting analysis revealed that NFATc1 in the nuclear fraction was increased in cells following stimulation with RANKL. When cells were incubated with both RANKL and curdlan, the level of NFATc1 protein in the nucleus was lower than in cells treated with RANKL alone (Fig. 9*C*).

*Curdlan Inhibits Osteoclastogenesis via Degradation of Syk Protein*—To clarify the role of Syk on osteoclastogenesis, we examined Syk expression in d-RAWs incubated with curdlan by immunoblot analysis. Surprisingly, time-dependent Syk degradation was observed in the presence of curdlan up to 3 h, whereas curdlan transiently phosphorylated Syk protein in d-RAWs from 15–60 min (Fig. 10*A*). By immunofluorescence analysis, d-RAWs, at all examined culture times, exhibited a background level of Syk that was localized primarily in the cytoplasm. Syk protein accumulation was also diminished by curdlan treatment up to 3 h (Fig. 10*B*). To confirm the involvement of Syk in osteoclast formation, d-RAWs were transfected with Syk siRNA and cultured with RANKL. Using Syk-specific siRNA transfected into d-RAWs, Syk mRNA was knocked down by ~50% compared with cells transfected with a nonspecific control siRNA (Fig. 10*C*). The knockdown of Syk protein was also confirmed by Western blot analysis (Fig. 10*D*). In d-RAWs transfected with control siRNA, RANKL-induced osteoclast formation was observed. However, in the Syk-specific siRNA-treated d-RAWs, osteoclast formation was diminished, even with RANKL treatment (Fig. 10, *E* and *F*). Furthermore, the RANKL-induced increase in NFATc1 expression was blocked in the presence of Syk siRNA (Fig. 10*G*).

*Inhibition of Syk Activation Abolished RANKL-induced Osteoclastogenesis*—To further substantiate the role of curdlan-dectin 1-Syk signaling in osteoclast formation induced by



FIGURE 8. **Effect of curdlan on RANKL-induced activation of osteoclast differentiation-related molecules in RAW cells.** c-RAWs and d-RAWs were incubated with or without curdlan (25 $\mu$g/ml) in the presence of RANKL (40 ng/ml) for the indicated time. Whole cell lysates were subjected to SDS-PAGE and Western blot analyses, with the blots probed for I$\kappa$B-$\alpha$ (*A*), phosphorylated c-jun (*phospho-c-jun*), c-jun (*B*) and c-fos (*C*). Equivalent protein aliquots of cell lysates were also analyzed for $\beta$-actin.

RANKL, d-RAWs were pretreated with the specific inhibitor for Syk. Two reagents, piceatannol and BAY 61-3606, are commonly used to block phosphorylation of Syk (31, 32). WST-1 analysis revealed that these inhibitors had no effect on d-RAW cell growth (data not shown) in the presence or absence of RANKL. Both piceatannol and BAY 61-3606 pretreatment effectively blocked RANKL-induced osteoclast formation in a dose-dependent manner (Fig. 11, *A–D*). Furthermore, the increase in NFATc1 expression, induced by RANKL, was decreased by pretreatment with both inhibitors (Fig. 11*E*).

## DISCUSSION

A number of studies have documented $\beta$-glucan modulation of biological activities in macrophages (11, 33, 34). Osteoclasts are large, multinucleated cells formed by the fusion of precursor cells in the monocyte/macrophage lineage (35). There is a considerable overlap of molecules and regulatory mechanisms shared between osseous and immune systems. With the aid of

99